

Sequential Bayesian inference for spatio-temporal models of temperature and humidity data

Yingying Lai

Andrew Golightly*

Richard Boys

School of Mathematics, Statistics and Physics, Newcastle University,
Newcastle upon Tyne, NE1 7RU, UK

Summary

We develop a spatio-temporal model to forecast sensor output at five locations in North East England. The signal is described using coupled dynamic linear models, with spatial effects specified by a Gaussian process. Data streams are analysed using a stochastic algorithm which sequentially approximates the parameter posterior through a series of reweighting and resampling steps. An iterated batch importance sampling scheme is used to circumvent particle degeneracy through a resample-move step. The algorithm is modified to make it more efficient and parallelisable. The model is shown to give a good description of the underlying process and provide reasonable forecast accuracy.

Keywords: Dynamic linear models (DLMs); sequential Monte Carlo (SMC); iterated batch importance sampling (IBIS); parallel computing.

1 Introduction

Climate is one of the most important environmental factors which plays a critical role on the global mission of urban sustainability. Consequently, it has attracted tremendous attention from academic scientists and industrial experts in recent decades. In this paper we focus on understanding the relationship between temperature and humidity, as these are two of the most important factors in driving other climate processes. Our primary objective is the development of dynamic models which can be used to understand the stochastic nature of temperature and humidity, as well as quantify their spatial dependencies. Moreover, in order to facilitate accurate forecasts in real time, we focus on developing algorithms which allow inferences to be made sequentially.

The literature contains several temporal models for temperature at a single location. For example, [1] proposed an autoregressive (AR) model with Fourier components to account for seasonality, a polynomial deterministic trend and a generalised autoregressive conditional heteroscedasticity (GARCH) error process. Further AR modelling approaches have been proposed by [2], [3] and [4], with the latter adopting a continuous-time approach. Although generic approaches for spatial data sets are widely available (see e.g. [5], [6], [7], [8], [9], [10] and [11]), relatively few papers have addressed the joint modelling of temperature and humidity at multiple locations. [12, 13] use a stochastic partial differential equation (SPDE) to model yearly temperature and humidity data at 120 locations and perform fully Bayesian inference via an integrated nested Laplace approximation [14].

The modelling approach developed here is motivated by the fine scale temporal nature of the available data. Dynamic linear models (DLMs) are widely used for system evolution learning and short term forecasting due to their simple and practical structures; see, for example, [15] for an

*email: andrew.golightly@ncl.ac.uk

introduction. We exploit these properties here by specifying a marginal DLM for temperature and a conditional DLM for humidity given temperature. We account for spatial dependence at nearby locations by adding a spatial Gaussian process to the system equations, thereby smoothing spatial deviations from the underlying temporal model. A similar approach was used by [16] for pollutant data.

We perform fully Bayesian inference for the model parameters as each observation becomes available. Since the posterior distribution is intractable, we use sequential Monte Carlo (SMC) methods that approximate the posterior distribution at each time point through a set of weighted samples; see [17] for a recent review of SMC methods. Although the posterior is intractable, the observed data likelihood is available in closed form, allowing the implementation of the iterated batch importance sampling (IBIS) scheme, first introduced by [18]; see also [19] for a related approach. Essentially, parameter samples (known in this context as particles) are incrementally weighted by the observed data likelihood contribution of the currently available observation. Particle degeneracy is mitigated via a resample-move step [20] which ‘moves’ each parameter particle through a Metropolis-Hastings kernel that leaves the target invariant. This step can be executed subject to the fulfilment of some degeneracy criterion e.g. small effective sample size. However, the computational cost of the resample-move step increases as the algorithm includes more data, as it requires calculation of the observed data likelihood of all available information. To obtain an online IBIS algorithm, where the computational cost of assimilating a single observation is bounded, we modify the resample-move step by basing the observed data likelihood on an observation window whose length is a tuning parameter, chosen to balance accuracy and computational efficiency. We use a simulation study to formulate practical advice on how to choose the size of this window.

Further computational savings can be made by employing a high performance computing system. Whilst the weighting and move steps can be performed independently for each particle, a basic implementation of the resampling step requires collective operations, such as adding up the particle weights. Our approach is to use a simple strategy which performs the resampling step independently for batches of parameter samples, thus allowing a fully parallel (per parameter batch) implementation of the algorithm to be performed. We quantify the effect of the approximation induced by this approach using synthetic data. Finally, we apply the online IBIS scheme (with parallel implementation) to the observed dataset and examine the model reliability and forecast accuracy through comparison of observed measurements with their posterior predictive distribution.

The remainder of the paper is organised as follows. A brief description of the data is given in Section 1.1. The structures of the spatial DLMs for temperature and humidity are discussed in Section 2. In Section 3, we introduce the IBIS scheme and develop a faster online version and then compare the performance of both schemes in Section 4 via a simulation study. In Section 5, we report the full analysis on our North East dataset on temperature and humidity and draw conclusions in Section 6.

1.1 Data collection

Recent advances in sensor technology and data management mean that it is now possible to reliably and affordably collect data on many aspects of city life. The temperature and relative humidity data analysed in this paper were collected from the Urban Observatory [21], a big data hub providing smart-city data via a grid of sensors in North East England. The data are received in real time, and this requires efficient network transmission and data storage solutions. Temperature is measured in degree Celsius, and relative humidity is measured as the ratio of the amount of water vapour held in the air against the the maximum amount of water vapour the air can hold at a specific temperature. The data are captured and processed through a microprocessor inside a sensor and transmitted via a high speed network to the database [22]. We consider data streams at five locations: Newcastle upon Tyne, Seaham, Peterlee, Whitley Bay and Consett. The observation period is from 8th July 2017 to 31st December 2017. Due to the different recording frequencies of some of the sensors, we

Variable	Location	Missing	Prop.	Mean	Min.	25%	Median	75%	Max.
Temperature (°C)	Newcastle	392	9.25%	10.62	-9.10	6.70	11.70	14.88	27.53
	Seaham	54	1.27%	11.48	-2.17	8.12	12.30	15.07	25.90
	Peterlee	46	1.09%	10.49	-2.24	7.37	11.52	13.95	22.68
	Whitley Bay	6	0.14%	11.07	-4.62	7.72	12.10	14.73	24.73
	Consett	306	7.22%	10.40	-3.37	6.90	11.20	14.24	24.38
Humidity (%)	Newcastle	392	9.25%	83.33	42.50	78.33	85.50	90.67	99.00
	Seaham	54	1.27%	73.62	34.23	67.08	74.50	81.67	97.42
	Peterlee	46	1.09%	84.86	44.83	80.22	86.83	91.67	99.00
	Whitley Bay	6	0.14%	86.25	50.00	82.25	88.25	93.00	98.25
	Consett	306	7.22%	83.59	46.40	79.33	86.00	90.50	97.00

Table 1: A summary of hourly average temperature and humidity data over the period 8th July 2017 to 31st December 2017 at five locations in North East England.

take the average values of temperature and relative humidity over every consecutive hour, giving a total of 4239 time points at which at least one location has a measurement. Figure 1 shows the multiple data streams over time at different locations. Both temperature and relative humidity exhibit a clear sinusoidal pattern over each 24 hour period. Scatter plots of humidity against temperature for each location are shown in Figure 2 and reveal a strong negative linear correlation. Unfortunately, missing data are inevitable due to network disconnection or sensor failure. Table 1.1 and Figure 1 summarise and display the proportion of missing data at each location during the observation period.

2 Spatial dynamic linear model (DLM)

We develop a joint model for hourly average temperature and humidity, recorded at each of L locations. The model is specified through a marginal model for temperature and a conditional model for humidity given temperature. Let $\mathbf{X}_{t_i} = (X_{t_i}^1, \dots, X_{t_i}^L)^T$ denote hourly average temperature taken over intervals $(t_i, t_{i+1}]$, with t_i in hours ($i = 1, \dots, n$) and $\mathbf{Y}_{t_i} = (Y_{t_i}^1, \dots, Y_{t_i}^L)^T$ denote the corresponding humidity values. In what follows we scale time so that $t_1 = 0$.

2.1 Spatial temperature DLM

In Section 1.1 we noted that the data show clear seasonality in both temperature and humidity measurements. This suggests that marginally each variable should be modelled by a sinusoidal form with a 24 hour period. For simplicity, consider first a single location j . We propose a DLM for temperature with observation equation

$$X_{t_i}^j = \mathbf{F}_{t_i}^{x,j} \boldsymbol{\theta}_{t_i}^{x,j} + v_i^{x,j}, \quad v_i^{x,j} \stackrel{\text{indep}}{\sim} N(0, V^{x,j}), \quad (1)$$

where the observation matrix $\mathbf{F}_{t_i}^{x,j} = (\cos(\pi t_i/12), \sin(\pi t_i/12), 1)$ and $\boldsymbol{\theta}_{t_i}^{x,j} = (\theta_{t_i,1}^{x,j}, \theta_{t_i,2}^{x,j}, \theta_{t_i,3}^{x,j})^T$. Note that, after dropping the superscripts for simplicity, the observation equation can be written as

$$X_{t_i} = \tilde{\theta}_{t_i,2} \cos\left(\frac{\pi t_i}{12} - \tilde{\theta}_{t_i,1}\right) + \theta_{t_i,3} + v_i \quad (2)$$

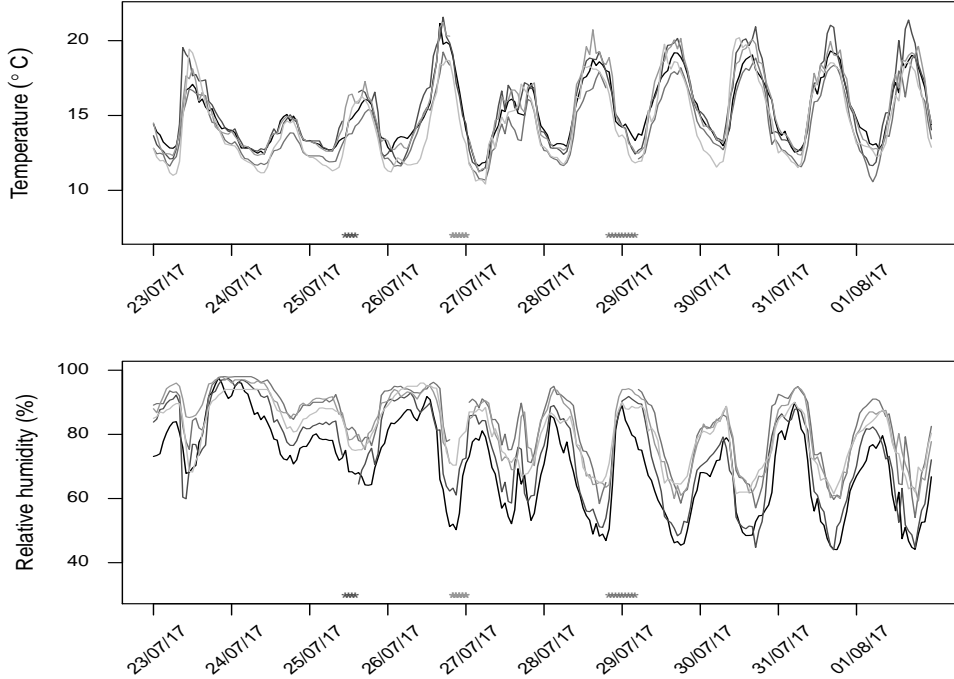


Figure 1: Temperature and relative humidity data streams over time at each location. Periods of missingness are indicated just above the x-axis.

where the parameters in (1) and (2) are related using

$$\tilde{\theta}_{t_i,1} = \sqrt{\theta_{t_i,1}^2 + \theta_{t_i,2}^2}, \quad \tilde{\theta}_{t_i,2} = \tan^{-1} \left(\frac{\theta_{t_i,2}}{\theta_{t_i,1}} \right). \quad (3)$$

We allow amplitude, phase shift and basal temperature to be time-varying, and take a system equation of the form

$$\boldsymbol{\theta}_{t_i}^{x,j} = \mathbf{G}_{t_i}^{x,j} \boldsymbol{\theta}_{t_{i-1}}^{x,j} + k_i \mathbf{w}_i^{x,j} + \mathbf{p}_i^{x,j}, \quad \mathbf{w}_i^{x,j} \stackrel{\text{indep}}{\sim} N \{ \mathbf{0}, \text{diag}(\mathbf{W}^{x,j}) \} \quad (4)$$

where the system matrix $\mathbf{G}_{t_i}^{x,j} = \mathbb{I}_3$, the 3×3 identity matrix, and $\mathbf{W}^{x,j} = (W_1^{x,j}, W_2^{x,j}, W_3^{x,j})^T$. Note that including k_i , where $k_i^2 = t_i - t_{i-1}$, allows for measurements to be on an irregularly spaced temporal grid. Further the terms $\mathbf{p}_i^{x,j} = (p_{i,1}^{x,j}, p_{i,2}^{x,j}, p_{i,3}^{x,j})^T$ allow for spatial variability between amplitude, phase shift and basal temperature values at nearby locations. We model the components of the spatially smooth error process $\mathbf{p}_i^{x,j}$ using independent zero mean Gaussian process (GP) priors with covariance functions $f_m^x(\cdot)$, $m = 1, 2, 3$, that is,

$$p_{i,m}^{x,j} \sim GP\{\mathbf{0}, f_m^x(\cdot)\}, \quad m = 1, 2, 3.$$

We take these covariance functions to have a simple exponential form

$$f_m^x(d_{jj'}) = \text{Cov}(\theta_{t_i,m}^{x,j}, \theta_{t_i,m}^{x,j'}) = \sigma_{x,m}^2 \exp(-\psi_{x,m} d_{jj'}), \quad m = 1, 2, 3$$

and depend on parameters $\boldsymbol{\sigma}_x = (\sigma_{x,1}, \sigma_{x,2}, \sigma_{x,3})$ and $\boldsymbol{\psi}_x = (\psi_{x,1}, \psi_{x,2}, \psi_{x,3})$, with the latter determining the decay ratio of the correlation as the distance between two locations $d_{jj'}$ increases [11].

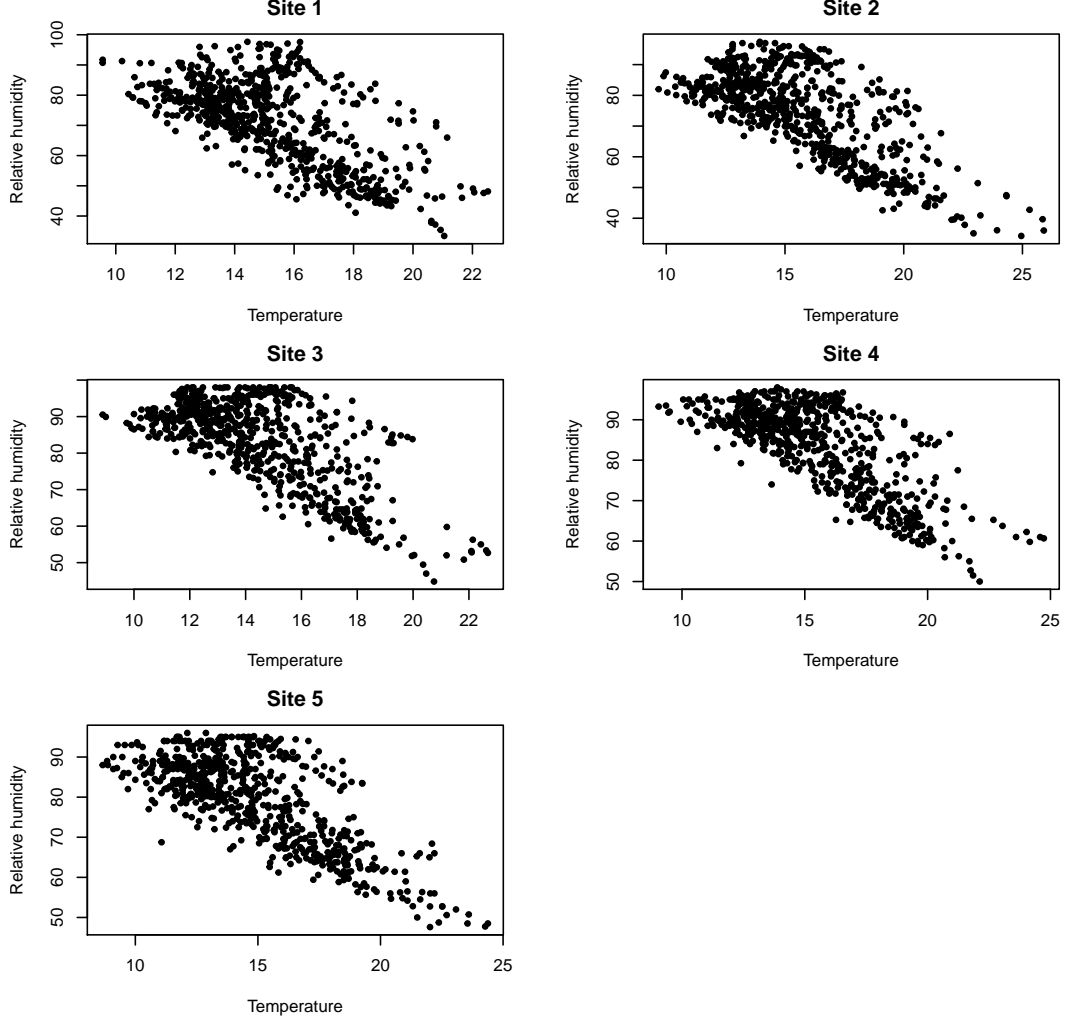


Figure 2: Scatter plots of temperature against relative humidity at each location.

The full spatial DLM model (over all locations) can be written as

$$\begin{aligned} \mathbf{X}_{t_i}^x &= \mathbf{F}_{t_i}^x \boldsymbol{\theta}_{t_i}^x + \mathbf{v}_i^x, & \mathbf{v}_i^x &\overset{\text{indep}}{\sim} N\{\mathbf{0}, \text{diag}(V^{x,1}, \dots, V^{x,\mathbb{L}})\}, \\ \boldsymbol{\theta}_{t_i}^x &= \boldsymbol{\theta}_{t_{i-1}}^x + k_i \mathbf{w}_i^x + \mathbf{p}_i^x, & \mathbf{w}_i^x &\overset{\text{indep}}{\sim} N\{\mathbf{0}, \text{diag}(W^{x,1}, \dots, W^{x,\mathbb{L}})\}, \end{aligned} \quad (5)$$

where $\mathbf{F}_{t_i}^x = \text{diag}(\mathbf{F}_{t_i}^{x,1}, \dots, \mathbf{F}_{t_i}^{x,\mathbb{L}})$, $\boldsymbol{\theta}_{t_i}^x = ((\boldsymbol{\theta}_{t_i}^{x,1})^T, \dots, (\boldsymbol{\theta}_{t_i}^{x,\mathbb{L}})^T)^T$ and the $3\mathbb{L}$ -vector of spatial effects $\mathbf{p}_i^x = ((\mathbf{p}_i^{x,1})^T, \dots, (\mathbf{p}_i^{x,\mathbb{L}})^T)^T$ is normally distributed with zero mean and covariance matrix

$$\mathbf{K}^x = \begin{pmatrix} f^x(d_{11})\mathbb{I}_3 & \dots & f^x(d_{1\mathbb{L}})\mathbb{I}_3 \\ \vdots & \ddots & \vdots \\ f^x(d_{\mathbb{L}1})\mathbb{I}_3 & \dots & f^x(d_{\mathbb{L}\mathbb{L}})\mathbb{I}_3 \end{pmatrix}.$$

2.1.1 Additional harmonics

Additional harmonics can be incorporated by using a Fourier form structure [see e.g. 15, 23]. For ease of exposition, we assume regularly spaced data at times $t_i = i-1$, $i = 1, \dots, n$. The observation matrix in (1) is defined to be the $1 \times (2q+1)$ matrix partitioned as $\mathbf{F}_{t_i}^{x,j} = (1, 0|1, 0|\dots|1)$ so that

the state vector $\boldsymbol{\theta}_{t_i}^{x,j}$ is of length $2q + 1$ and satisfies a system equation of the form (4) with system matrix $\mathbf{G}_{t_i}^{x,j} = \text{diag}(\mathbf{H}_1, \dots, \mathbf{H}_q, 1)$, where the \mathbf{H}_r are harmonic matrices

$$\mathbf{H}_r = \begin{pmatrix} \cos(\pi r/12) & \sin(\pi r/12) \\ -\sin(\pi r/12) & \cos(\pi r/12) \end{pmatrix}, \quad r = 1, \dots, q.$$

The number of harmonics q must be specified by the practitioner. Note that for the full spatial temperature DLM, specifying q harmonics will give $2L(q + 1) + 6$ static parameters to be inferred. Consequently, Fourier models with $q = 1$ or 2 are typically used in practice [23]. For the $q = 1$ harmonic and the trivial case of $\mathbf{W}^{x,j} = \mathbf{0}$, the observation equation of the Fourier form DLM coincides with that the sinusoidal form in (1) given by

$$X_{t_i}^j = \theta_{0,1}^{x,j} \cos(\pi t_i/12) + \theta_{0,2}^{x,j} \sin(\pi t_i/12) + \theta_{0,3}^{x,j} + v_i^{x,j}.$$

However, when $\mathbf{W}^{x,j} \neq \mathbf{0}$, the error structures differ due to the use of the harmonic in the system equation of the Fourier form DLM, and in the observation equation for the sinusoidal form DLM. The task of choosing between competing models is considered in Appendix A.3.

2.2 Spatial humidity DLM

Due to the strong linear relationship between temperature and humidity, we specify a conditional DLM for humidity by regressing on temperature in the observation equation. For a particular location j , the DLM takes the form

$$\begin{aligned} Y_{t_i}^j &= \mathbf{F}_{t_i}^{y,j} \boldsymbol{\theta}_{t_i}^{y,j} + v_i^{y,j}, & v_i^{y,j} &\stackrel{\text{indep}}{\sim} N(0, V^{y,j}) \\ \boldsymbol{\theta}_{t_i}^{y,j} &= \boldsymbol{\theta}_{t_{i-1}}^{y,j} + k_i \mathbf{w}_i^{y,j} + \mathbf{p}_i^{y,j}, & \mathbf{w}_i^{y,j} &\stackrel{\text{indep}}{\sim} N\{\mathbf{0}, \text{diag}(\mathbf{W}^{y,j})\} \end{aligned}$$

where $\mathbf{F}_{t_i}^{y,j} = (X_{t_i}^j, 1)$, $\boldsymbol{\theta}_{t_i}^{y,j} = (\theta_{t_i,1}^{y,j}, \theta_{t_i,2}^{y,j})^T$ and $\mathbf{W}^{y,j} = (W_1^{y,j}, W_2^{y,j})^T$. As in Section 2.1, we assign the components of the spatial error process $\mathbf{p}_i^{y,j} = (p_{i,1}^{y,j}, p_{i,2}^{y,j})^T$ independent zero mean Gaussian process priors with covariance functions

$$f_m^y(d_{jj'}) = \text{Cov}(\theta_{t_i,m}^{y,j}, \theta_{t_i,m}^{y,j'}) = \sigma_{y,m}^2 \exp(-\psi_{y,m} d_{jj'}), \quad m = 1, 2.$$

The spatial humidity DLM then takes the form

$$\begin{aligned} Y_{t_i} &= \mathbf{F}_{t_i}^y \boldsymbol{\theta}_{t_i}^y + v_i^y, & v_i^y &\stackrel{\text{indep}}{\sim} N\{\mathbf{0}, \text{diag}(V^{y,1}, \dots, V^{y,L})\} \\ \boldsymbol{\theta}_{t_i}^y &= \boldsymbol{\theta}_{t_{i-1}}^y + k_i \mathbf{w}_i^y + \mathbf{p}_i^y, & \mathbf{w}_i^y &\stackrel{\text{indep}}{\sim} N\{\mathbf{0}, \text{diag}(\mathbf{W}^{y,1}, \dots, \mathbf{W}^{y,L})\} \end{aligned} \quad (6)$$

where $\mathbf{F}_{t_i}^y = \text{diag}(\mathbf{F}_{t_i}^{y,1}, \dots, \mathbf{F}_{t_i}^{y,L})$, $\boldsymbol{\theta}_{t_i}^y = ((\theta_{t_i,1}^{y,1})^T, \dots, (\theta_{t_i,1}^{y,L})^T)^T$ and the $2L$ -vector of spatial effects \mathbf{p}_i^y is distributed analogously to \mathbf{p}_i^x . Note that the joint model given by (5) and (6) induces a marginal model for hourly average humidity with the sinusoidal pattern observed in the data. After integrating out $X_{t_i}^j$ in the observation equation for $Y_{t_i}^j$, we obtain

$$Y_{t_i}^j = \mathbf{F}_{t_i}^{x,j} \boldsymbol{\theta}_{t_i}^{x,j} \theta_{t_i,1}^{y,j} + \theta_{t_i,2}^{y,j} + v_i^{y,j} + \theta_{t_i,1}^{y,j} v_i^{x,j}$$

which exhibits the same sinusoidal structure of (1), albeit with a different amplitude, phase and basal level. It is clear that the joint model for $(X_{t_i}^j, Y_{t_i}^j)^T$ is not a DLM, as the marginal humidity model depends on $\boldsymbol{\theta}_{t_i}^{x,j}$ and $\boldsymbol{\theta}_{t_i}^{y,j}$ in a nonlinear way. Nevertheless, the factorisation of the joint model as marginal and conditional DLMs can be exploited when performing inference for the model parameters, and this is the subject of the next section.

3 Sequential Bayesian inference

3.1 Setup

Fitting the model for temperature and humidity described in Section 2 to data is complicated by the fact that in practice, sensor data is sometimes missing at one or more locations. To deal with this scenario, we let $\mathbf{X}_{t_i}^o$ and $\mathbf{Y}_{t_i}^o$ denote the observed temperature and humidity processes at time t_i . We assume that if temperature is missing at location j at time t_i , then so is humidity (and vice-versa), as is the case for our application. The observation model can then be written as

$$\mathbf{X}_{t_i}^o = \mathbf{P}_{t_i} \mathbf{X}_{t_i}, \quad \mathbf{Y}_{t_i}^o = \mathbf{P}_{t_i} \mathbf{Y}_{t_i} \quad (7)$$

where the $n_i \times \mathbb{L}$ incidence matrix \mathbf{P}_{t_i} determines which components are observed at time t_i . For example, if we have data streams from 5 different locations and data are missing at the second and third location at time t_i , then the incidence matrix is

$$\mathbf{P}_{t_i} = \begin{pmatrix} 1 & 0 & 0 & 0 & 0 \\ 0 & 0 & 0 & 1 & 0 \\ 0 & 0 & 0 & 0 & 1 \end{pmatrix}.$$

Let ϕ_x denote the flattened vector of $V^{x,1}, \dots, V^{x,\mathbb{L}}, \mathbf{W}^{x,1}, \dots, \mathbf{W}^{x,\mathbb{L}}, \sigma_x$ and ψ_x . Define ϕ_y similarly. Given observations $\mathbf{x}_{0:t_i}^o$ and $\mathbf{y}_{0:t_i}^o$ at times $0 = t_1 < t_2 < \dots < t_i$, our primary goal is sequential exploration of the marginal posterior density $\pi(\phi_x, \phi_y | \mathbf{x}_{0:t_i}^o, \mathbf{y}_{0:t_i}^o)$. We assume that ϕ_x and ϕ_y are independent *a priori* with prior density $\pi(\phi_x, \phi_y) = \pi(\phi_x)\pi(\phi_y)$. Bayes' theorem gives the posterior density of interest as

$$\begin{aligned} \pi(\phi_x, \phi_y | \mathbf{x}_{0:t_i}^o, \mathbf{y}_{0:t_i}^o) &\propto \pi(\phi_x)\pi(\phi_y)\pi(\mathbf{x}_{0:t_i}^o, \mathbf{y}_{0:t_i}^o | \phi_x, \phi_y) \\ &= \pi(\phi_x)\pi(\phi_y)\pi(\mathbf{x}_{0:t_i}^o | \phi_x)\pi(\mathbf{y}_{0:t_i}^o | \mathbf{x}_{0:t_i}^o, \phi_y) \\ &\propto \pi(\phi_x | \mathbf{x}_{0:t_i}^o)\pi(\phi_y | \mathbf{x}_{0:t_i}^o, \mathbf{y}_{0:t_i}^o) \end{aligned} \quad (8)$$

and so the parameter sets ϕ_x and ϕ_y are independent *a posteriori*. Moreover, we have that

$$\begin{aligned} \pi(\phi_x | \mathbf{x}_{0:t_i}^o) &\propto \pi(\phi_x | \mathbf{x}_{0:t_{i-1}}^o)\pi(\mathbf{x}_{0:t_i}^o | \mathbf{x}_{0:t_{i-1}}^o, \phi_x) \\ \pi(\phi_y | \mathbf{x}_{0:t_i}^o, \mathbf{y}_{0:t_i}^o) &\propto \pi(\phi_y | \mathbf{x}_{0:t_{i-1}}^o, \mathbf{y}_{0:t_{i-1}}^o)\pi(\mathbf{y}_{0:t_i}^o | \mathbf{x}_{0:t_i}^o, \mathbf{y}_{0:t_{i-1}}^o, \phi_y) \end{aligned} \quad (9)$$

where the observed data likelihood contributions $\pi(\mathbf{x}_{0:t_i}^o | \mathbf{x}_{0:t_{i-1}}^o, \phi_x)$ and $\pi(\mathbf{y}_{0:t_i}^o | \mathbf{x}_{0:t_i}^o, \mathbf{y}_{0:t_{i-1}}^o, \phi_y)$ can be calculated using a forward filter [15]. Details of this calculation can be found in Appendix A.1.

3.2 Iterated batch importance sampling

Although the parameter posterior is intractable, the form of (9) suggests a sequential importance sampling scheme that repeatedly reweights a set of N parameter samples (known as ‘particles’ in this context) by the observed data likelihood contributions. This approach is used in the iterated batch importance sampling (IBIS) algorithm of [18], together with MCMC steps for rejuvenating parameter samples in order to circumvent particle degeneracy. Given the factorisation of the posterior in (8), in what follows we focus on recursive sampling from $\pi(\phi_x | \mathbf{x}_{0:t_i}^o)$ and note that the steps for sampling from $\pi(\phi_y | \mathbf{x}_{0:t_i}^o, \mathbf{y}_{0:t_i}^o)$ are similar.

Suppose that a weighted sample $\{\phi_x^{(k)}, \omega_{t_i}^{(k)}\}_{k=1}^N$ from $\pi(\phi_x | \mathbf{x}_{0:t_i}^o)$ is available. The IBIS algorithm involves two steps: an incremental weighting step and a rejuvenation (resample-move) step. In the incremental weight step, the weight is updated for each particle through the observed data likelihood contribution of the current observation, i.e. $\omega_{t_i}^{(k)} \propto \omega_{t_{i-1}}^{(k)} \pi(\mathbf{x}_{0:t_i}^o | \mathbf{x}_{0:t_{i-1}}^o, \phi_x^{(k)})$. Note

that the calculation of the observed data likelihood increment (as given by the forward filter in Appendix A.1) requires the posterior summaries $\mathbf{m}_{t_{i-1}}(\phi_x^{(k)}) = \mathbf{m}_{t_{i-1}}^{(k)}$ and $\mathbf{C}_{t_{i-1}}(\phi_x^{(k)}) = \mathbf{C}_{t_{i-1}}^{(k)}$ of $\pi(\boldsymbol{\theta}_{t_i}^x | \mathbf{x}_{0:t_{i-1}}^o, \phi^x)$.

Simply updating the incremental weights over the time will lead to particle degeneracy. To bypass this problem, the IBIS scheme uses a resample-move step [see e.g. 20] that firstly resamples parameter particles (e.g. by drawing indices from a multinomial $\mathcal{M}(\omega^{1:N})$ distribution) and then moves each parameter sample through a Metropolis-Hastings kernel which leaves the target posterior invariant. The resample-move step is only used if some degeneracy criterion is fulfilled. Typically, at each time t_i , the effective sample size (ESS) is computed as

$$\text{ESS} = 1 / \sum_{k=1}^N (\omega_{t_i}^{(k)})^2$$

and the resample-move step is triggered if $\text{ESS} < \delta N$ for $\delta \in (0, 1)$ and a standard choice is $\delta = 0.5$. As the parameters must be strictly positive, we take a proposal density

$$q(\phi_x^* | \phi_x) = \log N \{ \phi_x^*; \log \phi_x, \gamma \text{Var}(\log \phi_x | \mathbf{x}_{0:t_i}^o) \}$$

where $\log N(\cdot; \mathbf{m}, \mathbf{V})$ denotes the density associated with the exponential of a $N(\mathbf{m}, \mathbf{V})$ random variable. We use the standard rule of thumb of [24] and [25] by taking the scaling parameter $\gamma = 2.38^2/n_{par}$, where n_{par} is the number of parameters. The full IBIS scheme is given by Algorithm 1.

Finally, we note that it is straightforward to estimate the evidence

$$\pi(\mathbf{x}_{0:t_n}^o) = \prod_{i=1}^n \pi(\mathbf{x}_{t_i}^o | \mathbf{x}_{0:t_{i-1}}^o)$$

using the output of the IBIS scheme, at virtually no additional computational cost. Each factor $L_{t_i} = \pi(\mathbf{x}_{t_i}^o | \mathbf{x}_{0:t_{i-1}}^o)$ in the product above is estimated by

$$L_{t_1} = \sum_{k=1}^N \frac{1}{N} \pi(\mathbf{x}_0^o | \phi_x^{(k)}), \quad L_{t_i} = \sum_{k=1}^N \omega_{t_{i-1}}^{(k)} \pi(\mathbf{x}_{t_i}^o | \mathbf{x}_{0:t_{i-1}}^o, \phi_x^{(k)}), \quad i = 2, \dots, n. \quad (10)$$

3.3 Online IBIS

The main computational bottleneck of IBIS is the resample-move step. If this step is triggered at time t_i , then the observed data likelihood $\pi(\mathbf{x}_{0:t_i}^o | \phi_x^*)$ must be calculated for each proposed particle ϕ_x^* . Consequently, the computational cost grows with t_i , precluding the use of IBIS as an online scheme. To bound the computational cost of assimilating a single observation, we modify the resample-move step by basing the observed data likelihood on an observation window whose time length is chosen to balance accuracy and computational efficiency.

We follow a similar approach introduced by [26] and define a sequence of windows with equal widths, say T , over the observation period. First the observation period is divided into b windows and denote by $\mathbf{x}_{t_i^s}^o$ the i th observation in window $s \in \{1, \dots, b\}$, for $i = 1, \dots, n_s$. The observation times satisfy $t_i^s \in ((s-1)T, sT]$ when $s = 1, \dots, b-1$ and $t_i^s \in ((b-1)T, t_{n_b}^b]$ when $s = b$. The standard IBIS scheme is run over the first window. For windows $s = 2, \dots, b$, the resample-move step targets

$$\tilde{\pi}(\phi_x | \mathbf{x}_{0:t_i^s}^o) \propto \tilde{\pi}(\phi_x | \mathbf{x}_{0:(s-1)T}) \pi(\mathbf{x}_{t_i^s:t_i^s}^o | \mathbf{x}_{0:(s-1)T}^o, \phi_x) \quad (11)$$

where

$$\tilde{\pi}(\phi_x | \mathbf{x}_{0:(s-1)T}) = \frac{1}{N} \sum_{k=1}^N \log N(\phi_x; \log \phi_x^{(k)}, h_s^2)$$

Algorithm 1 IBIS scheme

1. Initialisation. For $k = 1, \dots, N$ sample $\phi_x^{(k)} \sim \pi(\cdot)$ and set $\tilde{\omega}_0^{(k)} = \pi(\mathbf{x}_0^o | \phi_x^{(k)})$ using iteration $i = 1$ of the forward filter. Store $\mathbf{m}_{t_1}^{(k)}$ and $\mathbf{C}_{t_1}^{(k)}$.

For $i = 2, \dots, n$:

2. Sequential importance sampling. For $k = 1, \dots, N$:

- (a) Perform iteration i of the forward filter to obtain $\pi(\mathbf{x}_{t_i}^o | \mathbf{x}_{0:t_{i-1}}^o, \phi_x^{(k)})$, $\mathbf{m}_{t_i}^{(k)}$ and $\mathbf{C}_{t_i}^{(k)}$. Note the convention that $\pi(\mathbf{x}_0^o | \phi_x^{(k)}) = \pi(\mathbf{x}_0^o | \mathbf{x}_{0:t_1}^o, \phi_x^{(k)})$.
- (b) Update and normalise the importance weights using

$$\tilde{\omega}_{t_i}^{(k)} = \tilde{\omega}_{t_{i-1}}^{(k)} \pi(\mathbf{x}_{t_i}^o | \mathbf{x}_{0:t_{i-1}}^o, \phi_x^{(k)}), \quad \omega_{t_i}^{(k)} = \frac{\tilde{\omega}_{t_i}^{(k)}}{\sum_{j=1}^N \tilde{\omega}_{t_i}^{(j)}}$$

- (c) Update the observed data likelihood using

$$\pi(\mathbf{x}_{0:t_i}^o | \phi_x^{(k)}) = \pi(\mathbf{x}_{0:t_{i-1}}^o | \phi_x^{(k)}) \pi(\mathbf{x}_{t_i}^o | \mathbf{x}_{0:t_{i-1}}^o, \phi_x^{(k)}).$$

3. If $\text{ESS} < \delta N$ resample and move as follows. For $k = 1, \dots, N$:

- (a) Sample indices $a_k \sim \mathcal{M}(\omega^{1:N})$ and set $\{\phi_x^{(k)}, \tilde{\omega}_{t_i}^{(k)}\} := \{\phi_x^{(a_k)}, 1\}$, $\pi(\mathbf{x}_{0:t_i}^o | \phi_x^{(k)}) := \pi(\mathbf{x}_{0:t_i}^o | \phi_x^{(a_k)})$, $\mathbf{m}_{t_i}^{(k)} := \mathbf{m}_{t_i}^{(a_k)}$ and $\mathbf{C}_{t_i}^{(k)} := \mathbf{C}_{t_i}^{(a_k)}$.
- (b) Propose $\phi_x^* \sim q(\cdot | \phi_x^{(k)})$. Perform iterations $1, \dots, i$ of the forward filter to obtain $\pi(\mathbf{x}_{0:t_i}^o | \phi_x^*)$. With probability

$$\min \left\{ 1, \frac{\pi(\phi_x^*) \pi(\mathbf{x}_{0:t_i}^o | \phi_x^*)}{\pi(\phi_x^{(k)}) \pi(\mathbf{x}_{0:t_i}^o | \phi_x^{(k)})} \times \frac{q(\phi_x^{(k)} | \phi_x^*)}{q(\phi_x^* | \phi_x^{(k)})} \right\}$$

put $\phi_x^{(k)} := \phi_x^*$, $\pi(\mathbf{x}_{0:t_i}^o | \phi_x^{(k)}) := \pi(\mathbf{x}_{0:t_i}^o | \phi_x^*)$, $\mathbf{m}_{t_i}^{(k)} := \mathbf{m}_{t_i}^*$ and $\mathbf{C}_{t_i}^{(k)} := \mathbf{C}_{t_i}^*$.

is a kernel density estimate (KDE) of $\pi(\phi_x | \mathbf{x}_{0:(s-1)T})$ and the bandwidth h_s^2 can be calculated using, for example, Silverman's rule of thumb [27] as

$$h_s^2 = 1.06^2 N^{-2/5} \widehat{\text{Var}}(\phi_x^{(1:N)} | \mathbf{x}_{0:(s-1)T}^o).$$

Thus in order to evaluate (11), we need only evaluate the observed data likelihood contribution from the beginning of the current window until the current time. Furthermore, by taking the proposal density to be $q(\phi_x^* | \phi_x) = \tilde{\pi}(\phi_x^* | \mathbf{x}_{0:(s-1)T})$, the kernel density estimate need not be evaluated in the MH acceptance ratio. The choice of the window width has a direct influence on computational efficiency and posterior accuracy. A simulation study comparing IBIS and online IBIS for different window lengths is given in Section 4.2. The online IBIS scheme is summarised by Algorithm 2.

3.4 Parallelising the algorithm

The incremental weighting steps are readily parallelised in an SMC scheme. Additionally, for IBIS the move step can be performed independently for each particle. However, commonly used resampling schemes, such as the multinomial approach considered here, involve a collective operation

Algorithm 2 Online IBIS scheme

1. Initialisation. Divide the observed period into b windows, $s \in \{1, \dots, b\}$. Denote by t_i^s the i th observation time in window s , $i = 1, \dots, n_s$. For $s = 1$, implement the IBIS scheme (Algorithm 1). For $s = 2, \dots, b$ and $i = 1, \dots, n_s$:

2. Sequential importance sampling. For $k = 1, \dots, N$:

- (a) Perform iteration i (corresponding to time t_i^s) of the forward filter to obtain $\pi(\mathbf{x}_{t_i^s}^o | \mathbf{x}_{0:t_{i-1}^s}^o, \phi_x^{(k)})$, $\mathbf{m}_{t_i^s}^{(k)}$ and $\mathbf{C}_{t_i^s}^{(k)}$.
- (b) Update and normalise the importance weights using

$$\tilde{\omega}_{t_i^s}^{(k)} = \tilde{\omega}_{t_{i-1}^s}^{(k)} \pi(\mathbf{x}_{t_i^s}^o | \mathbf{x}_{0:t_{i-1}^s}^o, \phi_x^{(k)}), \quad \omega_{t_i^s}^{(k)} = \frac{\tilde{\omega}_{t_i^s}^{(k)}}{\sum_{z=1}^N \tilde{\omega}_{t_i^s}^{(z)}}$$

(c) Update the observed data likelihood contribution in the current window using

$$\pi(\mathbf{x}_{t_1^s:t_i^s}^o | \mathbf{x}_{0:(s-1)T}^o, \phi_x^{(k)}) = \pi(\mathbf{x}_{t_1^s:t_{i-1}^s}^o | \mathbf{x}_{0:(s-1)T}^o, \phi_x^{(k)}) \pi(\mathbf{x}_{t_i^s}^o | \mathbf{x}_{0:t_{i-1}^s}^o, \phi_x^{(k)}),$$

with the convention that $\pi(\mathbf{x}_{t_1^s:t_i^s}^o | \mathbf{x}_{0:(s-1)T}^o, \phi_x^{(k)}) = \pi(\mathbf{x}_{t_1^s}^o | \mathbf{x}_{0:(s-1)T}^o, \phi_x^{(k)})$ for $i = 1$.

3. If $\text{ESS} < \delta N$ resample and move. For $k = 1, \dots, N$:

- (a) Sample indices $a_k \sim \mathcal{M}(\omega^{1:N})$ and set $\{\phi_x^{(k)}, \tilde{\omega}_{t_i^s}^{(k)}\} := \{\phi_x^{(a_k)}, 1\}$, $\mathbf{m}_{t_i^s}^{(k)} := \mathbf{m}_{t_i^s}^{(a_k)}$, $\mathbf{C}_{t_i^s}^{(k)} := \mathbf{C}_{t_i^s}^{(a_k)}$ and $\pi(\mathbf{x}_{t_1^s:t_i^s}^o | \mathbf{x}_{0:(s-1)T}^o, \phi_x^{(k)}) := \pi(\mathbf{x}_{t_1^s:t_i^s}^o | \mathbf{x}_{0:(s-1)T}^o, \phi_x^{(a_k)})$.
- (b) Propose $\phi_x^* \sim \log N(\log \phi_x^{(k)}, h_s^2)$. Using $\mathbf{m}_{(s-1)T}^* = \mathbf{m}_{(s-1)T}^{(k)}$ and $\mathbf{C}_{(s-1)T}^* = \mathbf{C}_{(s-1)T}^{(k)}$, perform iterations $1, \dots, i$ (corresponding to times t_1^s, \dots, t_i^s) of the forward filter to obtain $\pi(\mathbf{x}_{t_1^s:t_i^s}^o | \mathbf{x}_{0:(s-1)T}^o, \phi_x^*)$. With probability

$$\min \left\{ 1, \frac{\pi(\mathbf{x}_{t_1^s:t_i^s}^o | \mathbf{x}_{0:(s-1)T}^o, \phi_x^*)}{\pi(\mathbf{x}_{t_1^s:t_i^s}^o | \mathbf{x}_{0:(s-1)T}^o, \phi_x^{(k)})} \right\}$$

put $\phi_x^{(k)} := \phi_x^*$, $\pi(\mathbf{x}_{t_1^s:t_i^s}^o | \mathbf{x}_{0:(s-1)T}^o, \phi_x^{(k)}) := \pi(\mathbf{x}_{t_1^s:t_i^s}^o | \mathbf{x}_{0:(s-1)T}^o, \phi_x^*)$, $\mathbf{m}_{t_i^s}^{(k)} := \mathbf{m}_{t_i^s}^*$ and $\mathbf{C}_{t_i^s}^{(k)} := \mathbf{C}_{t_i^s}^*$.

(summing the weights) precluding obvious parallelisation of the full IBIS scheme. [28] and [29] describe a forward adder tree method which parallelises the calculation of the cumulative weight. [30] suggest parallel Metropolis resampling and rejection resampling schemes to mitigate numerical instabilities of summing the weights for a large number of particles. However, these methods still require information exchange and global operations and they are designed mainly for use on GPU shared memory systems.

Distributed memory systems are naturally amenable to heavy parallelised jobs, where trunks of jobs are allocated and processed over multiple cores in different processors. In this context, a number of parallel resampling methods have been discussed in the literature; see, for example, [31] and [32, 33]. We follow the local resampling method [31] by partitioning particles into disjoint subsets, within which resampling is performed. The algorithm proceeds by first calculating a local ESS for each subset of particles. If a local ESS is less than a threshold, then the rejuvenation

step is triggered locally. The innovation variance for the MH proposal in the move step is also calculated locally based on the individual particle subset. To mitigate load-balance problems that can occur when the resample-move step is executed for some subsets but not others, we also carry out a rejuvenation step at regular time points, e.g. every 20 time points. This approach naturally fits within the distributed memory architecture and allows full parallelisation of the IBIS scheme. In principle, this approach should significantly improve computational efficiency of the inference scheme, as there is no need for task communication. However, in practice the number of informative particles may reduce significantly in some subsets as the algorithm runs. This in turn results in the rejuvenation step being executed more frequently. Therefore, a trade-off has to be considered carefully between the number of particle subsets and the number of particles in each subset. Section 4.1 describes a simulation study comparing a standard serial implementation with a fully parallelised version (with local resampling).

4 Simulation study

In order to assess the performance of the proposed online IBIS scheme and the effect of local resampling, we looked at results from synthetic data generated from the marginal model in (5). We consider 2 spatial locations (giving 14 parameters in total) and simulated $n = 1300$ observations at each location. The true parameter values used to produce the synthetic data are $W_k^j = 0.01$, $V^j = \sigma_k^2 = 1$ and $\psi_k = 0.01$ for $j = 1, 2$ and $k = 1, 2, 3$, and these values are shown in Figure 3. As this is a data-rich scenario, we assumed very weak independent inverse Gamma $IG(1, 0.01)$ prior distributions for all these parameter components, but truncated them above at 10 as values in excess of 10 are far from plausible. We also took the prior distribution for the initial system state as $\boldsymbol{\theta}_0 \sim N(\boldsymbol{m}, \boldsymbol{C})$, where $\boldsymbol{m} = (0, 0, 17, 0, 0, 17)^T$ and $\boldsymbol{C} = \mathbb{I}_6$. We used 10^7 particles and an ESS threshold of $\delta = 0.5$ for triggering the resample-move step. All computer code was written in C and executed on a high performance cluster with Intel Xeon E5-2699 v4 processors (2.2 GHz, 55 MB cache), where each processor has 22 cores (2.9 GB CPU memory per core).

4.1 Comparison of full IBIS with serial resampling and parallelised local resampling

We consider first two parallelised implementations of the full IBIS scheme: (i) weighting and move steps are performed in parallel over 22 cores through a shared memory system (within one processor) with the resampling step performed in serial; (ii) particles are divided over 200 cores and local resampling is used. Figure 3 shows the parameter marginal posterior densities obtained by using method 1 (IBIS with serial resampling) and method 2 (IBIS with parallelised local resampling). It is clear that both approaches give posterior output consistent with the true values (used to simulate the data). Moreover, the posterior densities from the fully parallelised method 2 match up well with those from the exact (simulation based) method 1. However the run time for method 1 (IBIS with serial resampling) is around 23 hours whereas that for method 2 (IBIS with parallelised local resampling) is around 4 hours, a speed-up of around a factor of 6.

4.2 Comparison of full IBIS and online IBIS

We now compare the full IBIS scheme with online IBIS and in both schemes we use the parallelised local resampling method. For online IBIS, we consider three widths for the fixed window: $T = 100$, 300 and 500. Figure 4 shows the output of the marginal posterior densities from the online IBIS scheme for each window size, together with the densities from the full IBIS scheme. As expected, as the larger window increases, so does posterior accuracy. The marginal posteriors from online IBIS using $T = 300$ and $T = 500$ almost overlay those from full IBIS. However, there are noticeable differences when using $T = 100$. In terms of computational efficiency, online IBIS with both

$T = 300$ and $T = 500$ take roughly 2 CPU hours, that with $T = 100$ takes approximately 1 CPU hour. Consequently, for this example, online IBIS with $T = 300$ and local parallel resampling gives an overall reduction in computational cost of around a factor of 12 compared to full IBIS with serial resampling.

5 Application

In this section we analyse the data on hourly average temperature and humidity values introduced in Section 1.1. Recall that these data are measurements recorded during the period 8th July 2017 to 31st December 2017 and that the observations are irregularly spaced due to network and sensor failures. We take independent inverse Gamma $IG(1, 0.01)$ prior distributions, truncated above at 10, for all the static parameters in both temperature and humidity DLMs. To incorporate our prior belief that the underlying system should be smoother than the observation process, we also impose the constraint that at each location $j = 1, \dots, 5$, $W_i^{x,j} < V^{x,j}$ ($i = 1, 2, 3$) and $W_k^{y,j} < V^{y,j}$ ($k = 1, 2$). We ran the online IBIS scheme with $N = 10^7$ particles, fully parallelised (with local resampling) over 200 cores using an ESS threshold of $\delta = 0.5$. Regular particle rejuvenation steps were set up for the process at every 20 time points, and the resample-move step was executed in any batch whose ESS fell below half the number of particles (in the batch). Finally, to balance accuracy and computational efficiency, we used a window width of $T = 1500$, and this gave a run time of approximately 9.5 days.

5.1 Inference results

Table 2 shows the marginal posterior medians and quantile-based 95% credible intervals for the static parameters in the joint temperature and humidity model. These summaries were obtained from output of the online IBIS scheme. Inspection of the posterior medians for the system variances (governing both temperature and humidity models) reveals that these components are larger at location 1 (Newcastle) than at the other locations. This is perhaps not surprising given that location 1 has the largest fraction of missing data (see Table 1.1). Also sampled posterior values of the observation variance components $V^{x,j}$ and $V^{y,j}$ are generally very much larger at location 2 (Seaham), and this too is consistent with the simple data summaries in Table 1.1 – Seaham is the least spatially consistent location in terms of median temperature and humidity. Variation across sites is accounted for by the elements of σ^2 . The relatively large values of $\sigma_{x,3}^2$ and $\sigma_{y,2}^2$ suggest that there is some spatial inconsistency in the dynamically varying mean level components $\theta_{t_i,3}^{x,j}$ and $\theta_{t_i,2}^{y,j}$. Spatial consistency of these mean level components can be assessed further by noting that

$$\text{Cor}(\theta_{t_i,3}^{x,j}, \theta_{t_i,3}^{x,j'}) = \exp(-\psi_{x,3} d_{jj'}), \quad \text{Cor}(\theta_{t_i,2}^{y,j}, \theta_{t_i,2}^{y,j'}) = \exp(-\psi_{y,2} d_{jj'}).$$

Hence, fixing $\psi_{x,3}$ and $\psi_{y,2}$ at their posterior medians gives a simple linear relationship between distance and log correlation. For example, within a 10km radius from each location, there is a spatial correlation of at least 0.76 for temperature and 0.64 for humidity. These areas are displayed in Figure 5. We note that it is not surprising that spatial correlation for humidity is lower than that for temperature, as the humidity records are also easily influenced by other factors, such as urban structure and distance from the sea, in addition to temperature.

5.2 Predictive performance

We assess the validity of the proposed model by comparing observed data with their model-based within-sample posterior predictive distributions and with model-based out-of-sample forecast distributions. Simulation methods can be used to construct these distributions and details on how to generate draws from them is provided in Appendix A.2. Figure 6 shows discrepancies between

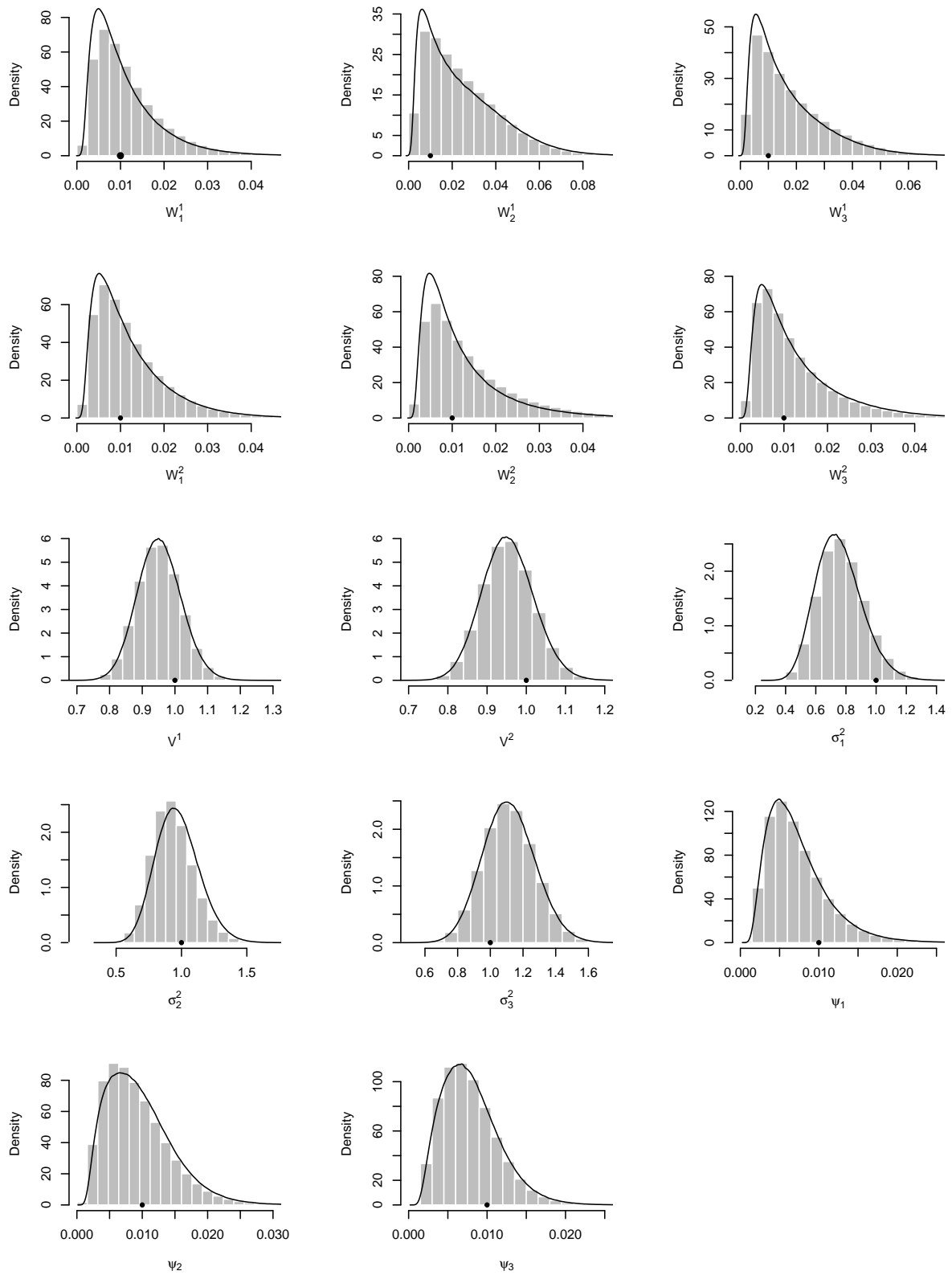


Figure 3: Marginal parameter posterior densities obtained from the output of the full IBIS scheme with a standard serial resampling step (histograms) and a parallelised local resampling step (—). The true parameter values are shown as solid circles.

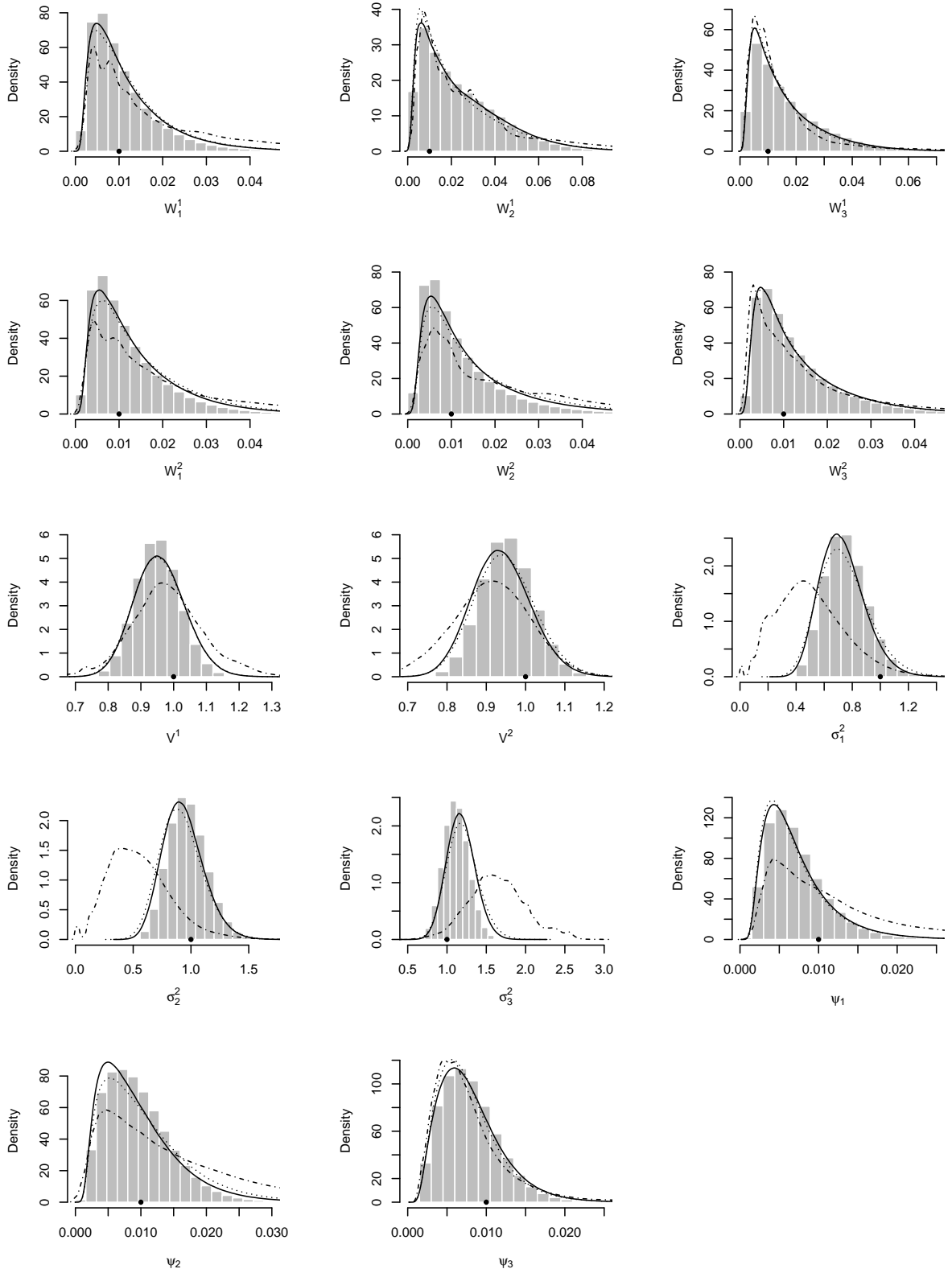


Figure 4: Marginal parameter posterior densities obtained from the output of the full IBIS scheme (histograms) and the online IBIS scheme with window widths $T = 100$ ($-\cdot-\cdot-$), $T = 300$ (\cdots) and $T = 500$ ($—$). The true parameter values are shown as solid circles.

Temperature				Humidity			
ϕ_x	Median	2.5%	97.5%	ϕ_y	Median	2.5%	97.5%
$W_1^{x,1}$	0.0050	0.0011	0.0110	$W_1^{y,1}$	0.0156	0.0118	0.0208
$W_2^{x,1}$	0.0056	0.0013	0.0114	$W_2^{y,1}$	0.0074	0.0019	0.0183
$W_3^{x,1}$	0.0053	0.0014	0.0116	$W_1^{y,2}$	0.0071	0.0049	0.0102
$W_1^{x,2}$	0.0026	0.0008	0.0089	$W_2^{y,2}$	0.0072	0.0018	0.0183
$W_2^{x,2}$	0.0031	0.0008	0.0095	$W_1^{y,3}$	0.0024	0.0014	0.0038
$W_3^{x,2}$	0.0039	0.0009	0.0096	$W_2^{y,3}$	0.0048	0.0015	0.0144
$W_1^{x,3}$	0.0021	0.0006	0.0082	$W_1^{y,4}$	0.0032	0.0017	0.0054
$W_2^{x,3}$	0.0023	0.0006	0.0075	$W_2^{y,4}$	0.0050	0.0016	0.0156
$W_3^{x,3}$	0.0021	0.0006	0.0083	$W_1^{y,5}$	0.0020	0.0010	0.0035
$W_1^{x,4}$	0.0027	0.0007	0.0083	$W_2^{y,5}$	0.0049	0.0016	0.0148
$W_2^{x,4}$	0.0032	0.0007	0.0095	$V^{y,1}$	0.0265	0.0147	0.0826
$W_3^{x,4}$	0.0036	0.0009	0.0102	$V^{y,2}$	0.4520	0.3362	0.5822
$W_1^{x,5}$	0.0042	0.0008	0.0103	$V^{y,3}$	0.0201	0.0137	0.0382
$W_2^{x,5}$	0.0026	0.0007	0.0089	$V^{y,4}$	0.0199	0.0137	0.0383
$W_3^{x,5}$	0.0038	0.0007	0.0092	$V^{y,5}$	0.0190	0.0134	0.0331
$V^{x,1}$	0.0089	0.0047	0.0173	$\sigma_{y,1}^2$	0.0257	0.0209	0.0315
$V^{x,2}$	0.0230	0.0110	0.0419	$\sigma_{y,2}^2$	1.6054	1.4961	1.7228
$V^{x,3}$	0.0078	0.0044	0.0138	$\psi_{y,1}$	0.0016	0.0008	0.0029
$V^{x,4}$	0.0088	0.0049	0.0251	$\psi_{y,2}$	0.0447	0.0388	0.0511
$V^{x,5}$	0.0164	0.0061	0.0380				
$\sigma_{x,1}^2$	0.0423	0.0105	0.1611				
$\sigma_{x,2}^2$	0.0627	0.0250	0.1672				
$\sigma_{x,3}^2$	0.2310	0.0837	0.2706				
$\psi_{x,1}$	0.0014	0.0004	0.0496				
$\psi_{x,2}$	0.0013	0.0004	0.0606				
$\psi_{x,3}$	0.0274	0.0011	0.0354				

Table 2: Marginal parameter posterior medians and quantile-based 95% credible intervals obtained from the output of the online IBIS scheme.

observations and their within-sample predictive distribution over the first 500 hours at each of the 5 locations. These distributions are characterised by their mean and 95% credible interval. It is clear that the mean difference at each time-location combination is small and that a mean difference of zero is plausible (the 95% credible intervals include zero). Similar results were obtained for the full data set (not shown). Figure 7 shows the mean and 95% credible interval at each location for the one-step ahead forecast. The times displayed were chosen at random over a two day period and, for comparison purposes, the observations at these times are also shown. Unsurprisingly forecast uncertainty grows during periods of prolonged missingness. The figure shows that observations typically lie within the forecast interval and that the model-based one-step forecast distribution is consistent with the observed data. Figure 8 shows the mean and 95% credible interval at each location for the two-step ahead forecast. Similar to the one-step forecasts, this figure shows that these forecast distributions are consistent with the data but, of course, have larger uncertainty.

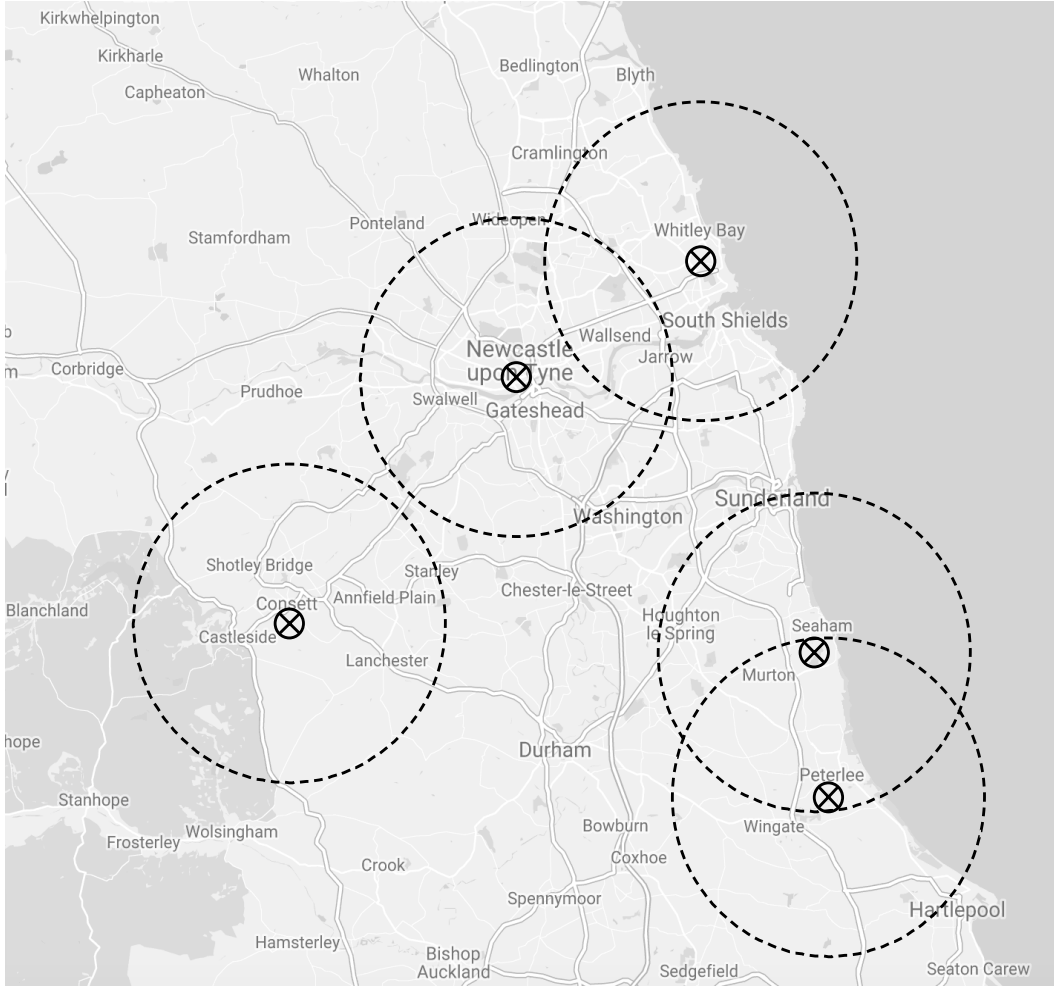


Figure 5: Map showing site locations and a 10 km radius from each site, within which the spatial correlation for temperature is at least 0.76, and for humidity, is at least 0.64.

6 Discussion

We have developed and fitted a spatio-temporal model to around six months of data on hourly temperature and humidity values at five locations in the North East of England. The data were obtained from a sensor network providing streaming data on environmental variables such as climate, pollution and traffic flow, held at the Newcastle Urban Observatory. The model we use for observed seasonality in temperature is a dynamic linear model (DLM) whose observation equation takes the form of a sinusoid, with time varying amplitude and phase described by the system equation. We capture the observed linear relationship between humidity and temperature via a conditional DLM in which humidity is regressed on temperature. Also spatial consistency at nearby sites is accounted for by adding a Gaussian process in the system equations.

Our primary goal is real time forecasting of temperature and humidity. To this end, we have developed a sequential Monte Carlo (SMC) algorithm which updates the parameter posterior as each measurement becomes available. The tractability of the observed data likelihood allows us to construct the SMC algorithm using an iterated batch importance sampling (IBIS) scheme, first introduced by [18]. The IBIS scheme tries to deal with particle degeneracy by employing a resample-move step which allows the particle set to be rejuvenated by moving each particle through a Metropolis-Hastings kernel that leaves the target posterior invariant. The computational cost of this step increases as the algorithm runs, due to the time taken to calculate the observed data

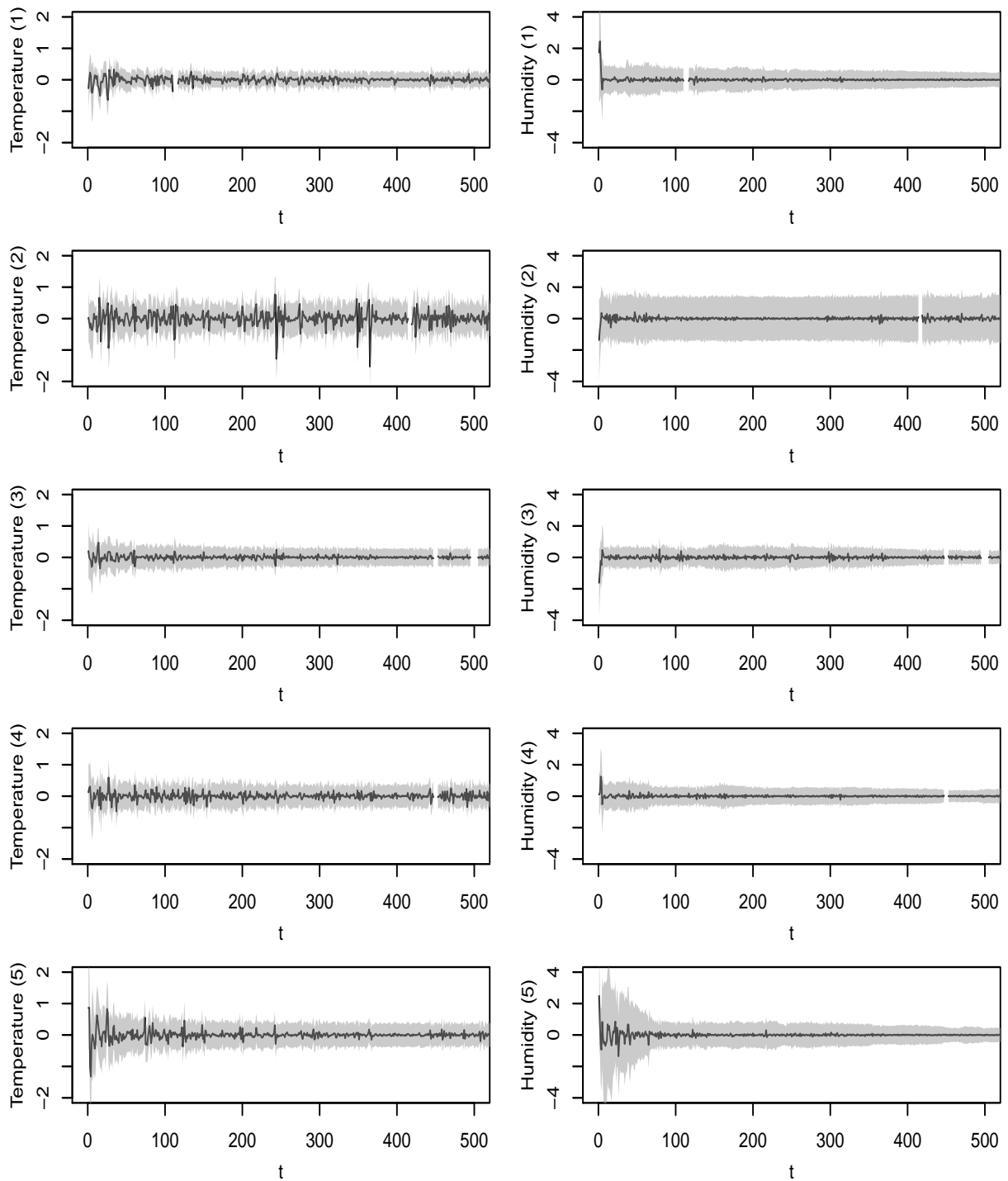


Figure 6: Mean (—) and 95% credible intervals for the difference between the within-sample predictive and the observations, at each location (1–5) over time. The observation period is from 8th July 2017 04:00:00 to 29th July 2017 00:00:00.

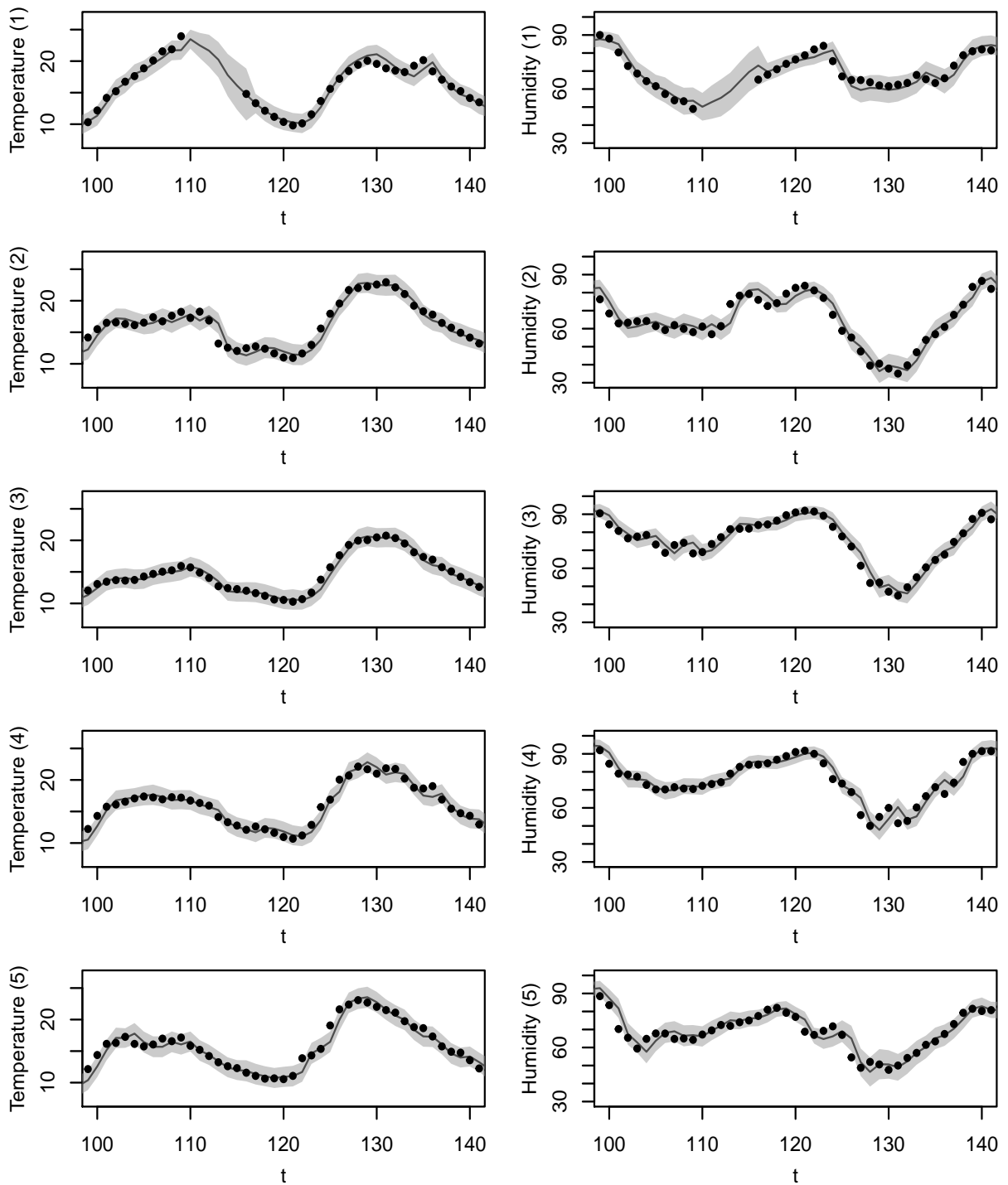


Figure 7: One-step ahead forecast means (—) and 95% credible intervals, at each location (1–5) over time. The observations are indicated (\bullet). The observation period is from 12th July 2017 08:00:00 to 14th July 2017 00:00:00.

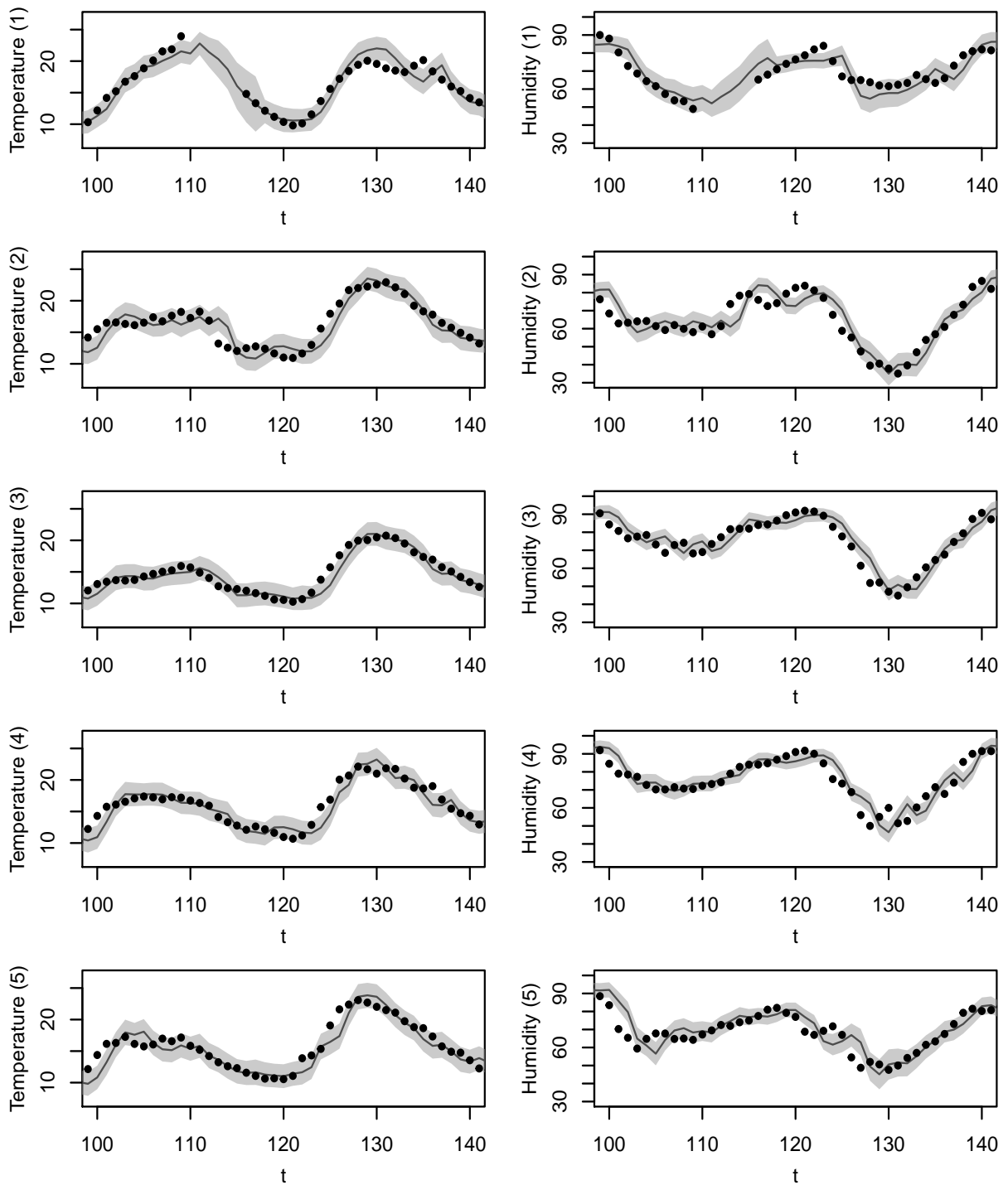


Figure 8: Two-step ahead forecast means (—) and 95% credible intervals, at each location (1–5) over time. The observations are indicated (\bullet). The observation period is from 12th July 2017 08:00:00 to 14th July 2017 00:00:00.

likelihood at each particle, as more data is included. This problem is made much more acute by the long length of the observed time series and the high dimension of the parameter space and this makes the algorithm unusable as an on-line algorithm. To circumvent this issue, we have modified the resample-move step in two ways. First, we use a sequence of observation windows and calculate the observed data likelihood for the data within the window. As the data in each window are included, the parameter posterior (at the start of the window) is approximated using a kernel density estimate and then updated using the observed data likelihood for the window. This places an upper bound on the computational cost. We looked the effect of the choice of window length on computational efficiency and posterior accuracy and found that reasonable posterior accuracy can be achieved for modest window length. Finally, we speed up the algorithm by using a fully parallel implementation which divides the particles into batches and performs the resampling step locally, for each batch. We term the resulting scheme *online IBIS* and find that for our data set, an observation (consisting of both temperature and humidity hourly averages at each of five locations) can be assimilated in around 3 minutes on average, with this average time dominated by the rejuvenation steps. One-step and two-step forecast distributions can then be determined very quickly. Given that observations arrive every hour, this makes the scheme entirely feasible for use in real time.

This work can be extended in a number of ways. For example, covariate information such as altitude, distance from the coast and wind direction/speed could be included in the model. Unfortunately this information is not currently available. Developing a joint model for all sensor streams, which would also include pollution data and traffic data, is also of interest. However, fitting models of multiple heterogeneous sensors is likely to require further methodological development of the inference scheme considered here.

References

- [1] S.D. Campbell and F.X. Diebold. Weather forecasting for weather derivatives. *Journal of the American Statistical Association*, 100:6–16, 2005.
- [2] W.K. Härdle and B.L. Cabrera. The implied market price of weather risk. *Applied Mathematical Finance*, 19:59–95, 2012.
- [3] F.E. Benth, J.S. Benth, and S. Koekebakker. Putting a price on temperature. *Scandinavian Journal of Statistics*, 34:746–767, 2007.
- [4] J.S. Benth and F.E. Benth. A critical view on temperature modelling for application in weather derivatives markets. *Energy Economics*, 34:592–602, 2012.
- [5] N. Cressie. *Statistics for Spatial Data*. Wiley-Interscience, 1993.
- [6] M.L. Stein. *Interpolation of Spatial Data: Some Theory for Kriging*. Springer, 1999.
- [7] B.D. Ripley. *Spatial Statistics*. Wiley-Interscience, 2004.
- [8] P. Diggle and P.J. Ribeiro. *Model-based Geostatistics*. Springer, 2004.
- [9] A.E. Gelfand, P. Diggle, M. Fuentes, and P. Guttorp. *Handbook of Spatial Statistics*. CRC Press, 2010.
- [10] N. Cressie and C.K. Wikle. *Statistics for Spatio-Temporal Data*. Wiley-Interscience, 2011.
- [11] S. Banerjee, B.P. Carlin, and A.E. Gelfand. *Hierarchical Modeling and Analysis for Spatial Data*. CRC Press, 2nd edition, 2014.

- [12] X. Hu, F. Lindgren, D. Simpson, and H. Rue. Multivariate Gaussian random fields with oscillating covariance functions using systems of stochastic partial differential equations. Available from <https://arxiv.org/abs/1307.1384>, 2013.
- [13] X. Hu, I. Steinsland, D. Simpson, S. Martino, and H. Rue. Spatial modelling of temperature and humidity using systems of stochastic partial differential equations. Available from <https://arxiv.org/abs/1307.1402>, 2015.
- [14] H. Rue, S. Martino, and N. Chopin. Approximate Bayesian inference for latent Gaussian models by using integrated nested Laplace approximations. *Journal of the Royal Statistical Society: Series B (Statistical Methodology)*, 71:319–392, 2009.
- [15] M. West and J. Harrison. *Bayesian Forecasting and Dynamic Models*. Springer, 2nd edition, 1999.
- [16] G. Shaddick and J. Wakefield. Modelling daily multivariate pollutant data at multiple sites. *J. R. Statist. Soc. C.*, 51:351–372, 2002.
- [17] P. Fearnhead and H. Künsch. Particle filters and data assimilation. Available from <https://arxiv.org/abs/1709.04196>, 2018.
- [18] N. Chopin. A sequential particle filter method for static models. *Biometrika*, 89:539–551, 2002.
- [19] N. Chopin, P.E. Jacob, and O. Papaspiliopoulos. SMC²: an efficient algorithm for sequential analysis of state space models. *J. R. Statist. Soc. B.*, 75:397–426, 2013.
- [20] W. R. Gilks and C. Berzuini. Following a moving target – Monte Carlo inference for dynamic Bayesian models. *J. R. Statist. Soc. B.*, 63:127–146, 2001.
- [21] P.M. James, R.J. Dawson, N. Harris, and J. Jonczyk. Urban Observatory Environment. Newcastle University. <http://dx.doi.org/10.17634/154300-19>. 2014.
- [22] F. Galatioto, M.C. Bell, and G. Hill. Understanding the characteristics of the microenvironments in urban street canyons through analysis of pollution measured using a novel pervasive sensor array. *Environmental Monitoring and Assessment*, 186:7443–7460, 2014.
- [23] G. Petris, S. Petrone, and P. Campagnoli. *Dynamic Linear Models with R*. Springer, 2009.
- [24] G.O. Roberts, A. Gelman, and W.R. Gilks. Weak convergence and optimal scaling of random walk Metropolis algorithms. *The Annals of Applied Probability*, 7:110–120, 1997.
- [25] G.O. Roberts and J.S. Rosenthal. Optimal scaling for various Metropolis-Hastings algorithms. *Statistical Science*, 16:351–367, 2001.
- [26] P. Del Moral, A. Jasra, and Y. Zhou. Biased online parameter inference for state-space models. *Methodology and Computing in Applied Probability*, 19:727–749, 2017.
- [27] B.W. Silverman. *Density Estimation for Statistics and Data Analysis*. Chapman & Hall/CRC, 1986.
- [28] G. Hendeby, R. Karlsson, and F. Gustafsson. Particle filtering: The need for speed. *EURASIP Journal on Advances in Signal Processing*, pages 1–9, 2010.
- [29] P. Gong, Y. Basciftci, and F. Ozguner. A parallel resampling algorithm for particle filtering on shared-memory architectures. 2012 IEEE 26th International Parallel and Distributed Processing Symposium Workshops and PhD Forum, pages 1477–1483, 2012.

- [30] L.M. Murray, A. Lee, and P.E. Jacob. Parallel resampling in the particle filter. *Journal of Computational and Graphical Statistics*, 25:789–805, 2016.
- [31] O. Brun, V. Teuliere, and J.M. Garcia. Parallel particle filtering. *Journal of Parallel and Distributed Computing*, 62:1186–1202, 2002.
- [32] M. Bolić, P.M. Djurić, and S. Hong. Resampling algorithms for particle filters: A computational complexity perspective. *EURASIP Journal on Advances in Signal Processing*, 15:2267–2277, 2004.
- [33] M. Bolić, P.M. Djurić, and S. Hong. Resampling algorithms and architectures for distributed particle filters. *IEEE Transactions on Signal Processing*, 53:2442–2450, 2005.
- [34] R. E. Kass and A. E. Raftery. Bayes factors. *Journal of the American Statistical Association*, 90:773–795, 1995.
- [35] S. Frühwirth-Schnatter. Bayesian model discrimination and Bayes factors for linear Gaussian state space models. *Journal of the Royal Statistical Society, Series B*, 57:237–246, 1995.

A Appendix

A.1 Forward filter

To simplify notation we consider the spatial temperature model and drop x . Given the form of the observation model in (7), we have that

$$\begin{aligned} \mathbf{X}_{t_i}^o &= \tilde{\mathbf{F}}_{t_i} \boldsymbol{\theta}_{t_i} + \tilde{\mathbf{v}}_i, & \tilde{\mathbf{v}}_i &\stackrel{\text{indep}}{\sim} N(\mathbf{0}, \tilde{\mathbf{V}}), \\ \boldsymbol{\theta}_{t_i} &= \boldsymbol{\theta}_{t_{i-1}} + \tilde{\mathbf{w}}_i, & \tilde{\mathbf{w}}_i &\stackrel{\text{indep}}{\sim} N(\mathbf{0}, \tilde{\mathbf{W}}), \end{aligned} \quad (12)$$

where $\tilde{\mathbf{F}}_{t_i} = \mathbf{P}_{t_i} \mathbf{F}_{t_i}$, $\tilde{\mathbf{V}} = \mathbf{P}_{t_i} \text{diag}(V^1, \dots, V^L) \mathbf{P}_{t_i}^T$ and $\tilde{\mathbf{W}} = k_i^2 \text{diag}(\mathbf{W}^1, \dots, \mathbf{W}^L) + \mathbf{K}$. Since the parameters $\boldsymbol{\phi}$ remain fixed throughout this section, we drop them from the notation where possible. Now suppose that $\boldsymbol{\theta}_{t_1} \sim N(\mathbf{m}, \mathbf{C})$ *a priori* and recall that $t_1 = 0$. The observed data likelihood increments $\pi(\mathbf{x}_{t_i}^o | \mathbf{x}_{0:t_{i-1}}^o)$, and hence the full observed data likelihood $\pi(\mathbf{x}_{0:t_n}^o | \boldsymbol{\phi})$, can be obtained from the forward filter described in Algorithm 3.

A.2 Within-sample predictions and out-of-sample forecasts

In order to compute within-sample predictions, the smoothing density $\pi(\boldsymbol{\theta}_{0:t_n} | \mathbf{x}_{0:t_n}^o, \boldsymbol{\phi}_x)$ is required. Draws from this density can be readily obtained by using a backward sampler that recursively draws from

$$\pi(\boldsymbol{\theta}_{t_i} | \boldsymbol{\theta}_{t_{i+1}}, \mathbf{x}_{0:t_i}^o, \boldsymbol{\phi}_x) = N\{\boldsymbol{\theta}_{t_i}; \mathbf{m}_{t_i} + \mathbf{B}_{t_i}(\boldsymbol{\theta}_{t_{i+1}} - \mathbf{m}_{t_i}), \mathbf{C}_{t_i} - \mathbf{B}_{t_i} \mathbf{R}_{t_{i+1}} \mathbf{B}_{t_i}^T\}, \quad (13)$$

where $\mathbf{B}_{t_i} = \mathbf{C}_{t_i} \mathbf{R}_{t_{i+1}}^{-1}$ and $\mathbf{R}_{t_{i+1}} = \mathbf{C}_{t_i} + \tilde{\mathbf{W}}$; see, for example, [15]. Hence, given an equally weighted sample $\{\boldsymbol{\phi}_x^{1:N}\}$ from the marginal posterior $\pi(\boldsymbol{\phi}_x | \mathbf{x}_{0:t_n}^o)$, we can integrate over parameter uncertainty to generate draws from the within-sample system posterior predictive density $\pi(\boldsymbol{\theta}_{0:t_n} | \mathbf{x}_{0:t_n}^o)$ by recursively drawing from (13) for each particle $\boldsymbol{\phi}_x^{(k)}$ (and the associated quantities $\mathbf{m}_{t_i}^{(k)}$, $\mathbf{C}_{t_i}^{(k)}$ generated by the forward filter). Subsequently, the within-sample observation posterior predictive density $\pi(\mathbf{x}_{0:t_n} | \mathbf{x}_{0:t_n}^o)$ can be sampled by drawing

$$\mathbf{X}_{t_i}^{(k)} | \boldsymbol{\theta}_{t_i}^{(k)}, \boldsymbol{\phi}_x^{(k)} \sim N(\mathbf{F}_{t_i} \boldsymbol{\theta}_{t_i}^{(k)}, \mathbf{V}^{(k)}), \quad i = 1, \dots, n, \quad k = 1, \dots, N.$$

Algorithm 3 Forward filter

1. Initialisation ($i = 1$). Compute $\pi(\mathbf{x}_{t_1}^o) = N(\mathbf{x}_{t_1}; \tilde{\mathbf{F}}_{t_1} \mathbf{m}, \tilde{\mathbf{F}}_{t_1} \mathbf{C} \tilde{\mathbf{F}}_{t_1}^T + \tilde{\mathbf{V}})$. The posterior at time $t_1 = 0$ is therefore $\boldsymbol{\theta}_{t_1} | \mathbf{x}_{t_1}^o \sim N(\mathbf{m}_{t_1}, \mathbf{C}_{t_1})$, where

$$\begin{aligned} \mathbf{m}_{t_1} &= \mathbf{m} + \mathbf{C} \tilde{\mathbf{F}}_{t_1}^T (\tilde{\mathbf{F}}_{t_1} \mathbf{C} \tilde{\mathbf{F}}_{t_1}^T + \tilde{\mathbf{V}})^{-1} (\mathbf{x}_{t_1}^o - \tilde{\mathbf{F}}_{t_1} \mathbf{m}) \\ \mathbf{C}_{t_1} &= \mathbf{C} - \mathbf{C} \tilde{\mathbf{F}}_{t_1}^T (\tilde{\mathbf{F}}_{t_1} \mathbf{C} \tilde{\mathbf{F}}_{t_1}^T + \tilde{\mathbf{V}})^{-1} \tilde{\mathbf{F}}_{t_1} \mathbf{C}. \end{aligned}$$

Store the values of \mathbf{m}_{t_1} , \mathbf{C}_{t_1} and $\pi(\mathbf{x}_{t_1}^o)$.

2. For $i = 2, \dots, n$,

- (a) Prior at t_i . Using the system equation, we have that $\boldsymbol{\theta}_{t_i} | \mathbf{x}_{0:t_{i-1}}^o \sim N(\mathbf{m}_{t_{i-1}}, \mathbf{C}_{t_{i-1}} + \tilde{\mathbf{W}})$.
 (b) One step forecast. Using the observation equation, we have that

$$\mathbf{X}_{t_i}^o | \mathbf{x}_{0:t_{i-1}}^o \sim N\{\tilde{\mathbf{F}}_{t_i} \mathbf{m}_{t_{i-1}}, \tilde{\mathbf{F}}_{t_i} (\mathbf{C}_{t_{i-1}} + \tilde{\mathbf{W}}) \tilde{\mathbf{F}}_{t_i}^T + \tilde{\mathbf{V}}\}.$$

Compute the observed data likelihood increment

$$\pi(\mathbf{x}_{t_i}^o | \mathbf{x}_{0:t_{i-1}}^o) = N\{\mathbf{x}_{t_i}^o; \tilde{\mathbf{F}}_{t_i} \mathbf{m}_{t_{i-1}}, \tilde{\mathbf{F}}_{t_i} (\mathbf{C}_{t_{i-1}} + \tilde{\mathbf{W}}) \tilde{\mathbf{F}}_{t_i}^T + \tilde{\mathbf{V}}\}.$$

- (c) Posterior at t_i . Combining the distributions in (a) and (b) gives the joint distribution of $\boldsymbol{\theta}_{t_i}$ and $\mathbf{X}_{t_i}^o$ (conditional on $\mathbf{x}_{0:t_{i-1}}^o$) as

$$\begin{pmatrix} \boldsymbol{\theta}_{t_i} \\ \mathbf{X}_{t_i}^o \end{pmatrix} \sim N \left\{ \begin{pmatrix} \mathbf{m}_{t_{i-1}} \\ \tilde{\mathbf{F}}_{t_i} \mathbf{m}_{t_{i-1}} \end{pmatrix}, \begin{pmatrix} \mathbf{C}_{t_{i-1}} + \tilde{\mathbf{W}} & (\mathbf{C}_{t_{i-1}} + \tilde{\mathbf{W}}) \tilde{\mathbf{F}}_{t_i}^T \\ \tilde{\mathbf{F}}_{t_i} (\mathbf{C}_{t_{i-1}} + \tilde{\mathbf{W}}) & \tilde{\mathbf{F}}_{t_i} (\mathbf{C}_{t_{i-1}} + \tilde{\mathbf{W}}) \tilde{\mathbf{F}}_{t_i}^T + \tilde{\mathbf{V}} \end{pmatrix} \right\}$$

and therefore $\boldsymbol{\theta}_{t_i} | \mathbf{x}_{0:t_i}^o \sim N(\mathbf{m}_{t_i}, \mathbf{C}_{t_i})$, where

$$\begin{aligned} \mathbf{m}_{t_i} &= \mathbf{m}_{t_{i-1}} + (\mathbf{C}_{t_{i-1}} + \tilde{\mathbf{W}}) \tilde{\mathbf{F}}_{t_i}^T \{ \tilde{\mathbf{F}}_{t_i} (\mathbf{C}_{t_{i-1}} + \tilde{\mathbf{W}}) \tilde{\mathbf{F}}_{t_i}^T + \tilde{\mathbf{V}} \}^{-1} (\mathbf{x}_{t_i}^o - \tilde{\mathbf{F}}_{t_i} \mathbf{m}_{t_{i-1}}) \\ \mathbf{C}_{t_i} &= \mathbf{C}_{t_{i-1}} + \tilde{\mathbf{W}} - (\mathbf{C}_{t_{i-1}} + \tilde{\mathbf{W}}) \tilde{\mathbf{F}}_{t_i}^T \{ \tilde{\mathbf{F}}_{t_i} (\mathbf{C}_{t_{i-1}} + \tilde{\mathbf{W}}) \tilde{\mathbf{F}}_{t_i}^T + \tilde{\mathbf{V}} \}^{-1} \tilde{\mathbf{F}}_{t_i} (\mathbf{C}_{t_{i-1}} + \tilde{\mathbf{W}}). \end{aligned}$$

Store the values of \mathbf{m}_{t_i} , \mathbf{C}_{t_i} and $\pi(\mathbf{x}_{t_i}^o | \mathbf{x}_{0:t_{i-1}}^o)$.

Out-of-sample system and observation forecast distributions can be obtained by again exploiting the linear Gaussian structure of the DLM. Given an equally weighted sample $\{\phi_x^{1:N}\}$ from the marginal posterior $\pi(\phi_x | \mathbf{x}_{0:t_n}^o)$, samples from $\pi(\boldsymbol{\theta}_{t_{n+1}} | \mathbf{x}_{0:t_n}^o)$ and $\pi(\mathbf{x}_{t_{n+1}} | \mathbf{x}_{0:t_n}^o)$ can be obtained by recursively drawing

$$\begin{aligned} \boldsymbol{\theta}_{t_{n+1}}^{(k)} | \phi_x^{(k)} &\sim N(\mathbf{m}_{t_n}^{(k)}, \mathbf{C}_{t_n}^{(k)} + \tilde{\mathbf{W}}^{(k)}), \quad k = 1, \dots, n \\ \mathbf{x}_{t_{n+1}}^{(k)} | \phi_x^{(k)} &\sim N\{\mathbf{F}_{t_{n+1}} \mathbf{m}_{t_n}^{(k)}, \mathbf{F}_{t_{n+1}} (\mathbf{C}_{t_n}^{(k)} + \tilde{\mathbf{W}}^{(k)}) \mathbf{F}_{t_{n+1}}^T + \mathbf{V}^{(k)}\}, \quad k = 1, \dots, n. \end{aligned}$$

A.3 Model selection

As noted in Section 2.1, seasonality in the marginal DLM can be accounted for in two ways. A sinusoid can be specified in the observation equation, with a system equation describing the evolution of the parameters governing the amplitude and phase. Alternatively, a Fourier form structure can be used in the system equation where the appropriate number of harmonics must be specified by the practitioner. Our joint model consists of a marginal DLM for temperature and a conditional DLM for humidity given temperature. This induces a marginal DLM for humidity

with the same form as that for temperature. We therefore consider three candidate spatial DLMs for modelling temperature and humidity data marginally: 1. sinusoidal form DLM (sDLM); 2. Fourier form DLM with 1 harmonic (FDLM1); 3. Fourier form DLM with 2 harmonics (FDLM2). Choosing between these competing models is possible via computation of the Bayes factor [34, 35], which, under the assumption of equal prior probability for two competing models, say $M1$ and $M2$, is defined as the ratio of the evidence given $M1$, and that given $M2$. The Bayes factor based on temperature data is therefore

$$BF = \frac{p(\mathbf{x}_{0:t_n}^o | M1)}{p(\mathbf{x}_{0:t_n}^o | M2)}$$

with a similar form for the humidity data Bayes factor. Note that $BF < 1$ suggests the data support $M2$. Equation (10) gives an estimate of the evidence as a by-product of the IBIS scheme.

Unfortunately, the size of the observed dataset precludes calculation of the Bayes factor using all measurements at all sites. Therefore, to guide our modelling approach we chose three of the five locations at random and then 400 consecutive observations (starting at a random observed time) at these locations. The evidence for each model was determined using the full IBIS scheme on these data with a serial multinomial resampling step for each model, using $N = 10^7$ particles. To account for Monte Carlo error, we repeat this process 30 times. Taking FDLM2 as a baseline for comparison, we compute Bayes factors for sDLM vs FDLM2 and FDLM1 vs FDLM2. Figure 9 shows the mean $\log BF$ value (and 95% credible interval) based on data $\mathbf{x}_{0:t}^o$ and $\mathbf{y}_{0:t}^o$ against t . For the marginal temperature DLM it is clear that FDLM2 is the least favoured model. Furthermore, for $t > 80$, the log Bayes factors corresponding to the sinusoidal form DLM against FDLM2 are always strictly greater than those corresponding to FDLM1 against FDLM2. For the marginal humidity DLM, there is little difference in overall fit between the sinusoidal form DLM and FDLM1. Given that computational cost scales as 1 : 1.1 : 1.3 for DLM : $FDLM1$: $FDLM2$, we conclude that the sinusoidal form DLM offers the best compromise between model fit and computational efficiency.

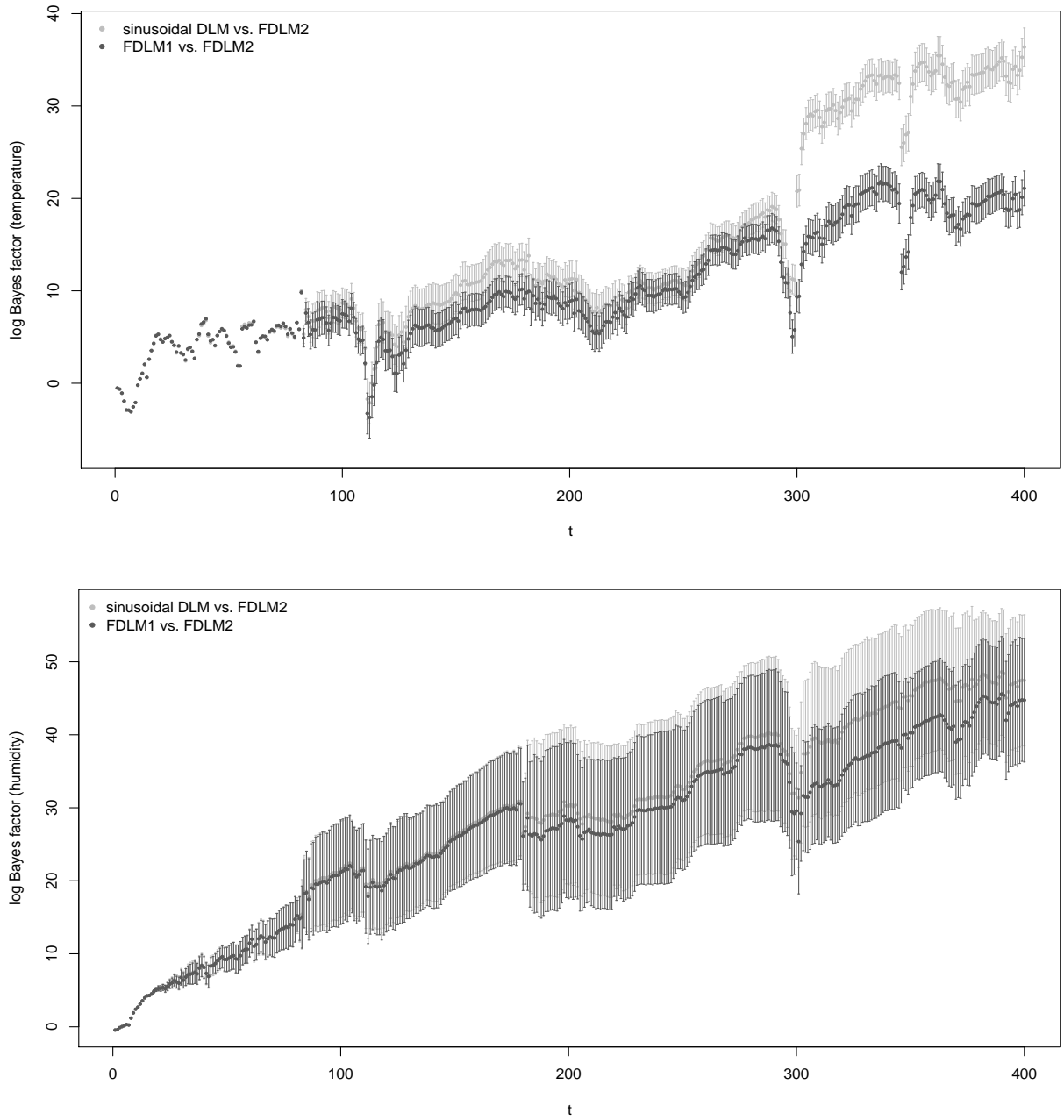


Figure 9: Mean and 95% credible interval of the log Bayes factor comparing sDLM against FDLM2 and FDLM1 against FDLM2, over time. (Top: temperature models; bottom: humidity models.)